Deanship of Graduate Studies

AL-Quds University

FINE STRUCTURE IN EXCITON-MAGNON BANDS IN Mn^{2+} MAGNETS

HAZEM KHALEEL WDAA'H SALAH

M.Sc. THESIS

Fine Structure in Exciton-Magnon Bands in Mn^{2+} Magnets

BY

Hazem Khaleel Wdaa'h Salah

(B.Sc. Physics, AL-Quds University)

Supervised By:

Saker Darwish, Ph.D.

Amin Leghrouz, Ph.D.

"Thesis Submitted to the College of Science and Technology of AL-Quds University in Partial Fulfillment of the Requirements for the Degree of Master of Science in Physics"

Abu-Dies, AL-Quds

Palestine

September, 2001

Fine Structure in Exciton-Magnon Bands in Mn^{2+} Magnets

Student Name: Hazem Khaleel Wdaa'h Salah.

Thesis Submitted for Examination on Tuesday 4, September 2001 and accepted by the examining committee formed of the following:

Committee Members	Signature
Edward Sader, Ph. D. (External Examiner)	
Amin Leghrous, Ph. D. (Internal Examiner)	
Saker Darwish, Ph. D. (Chairman)	

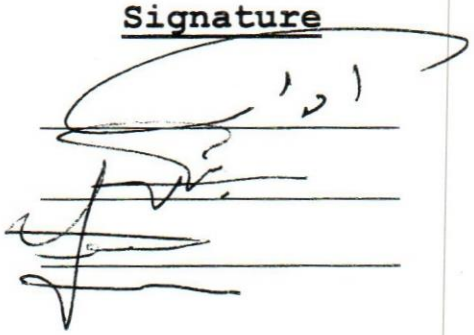

Al-Quds University

2001

بسم الله الرحمن الرحيم

"وما توفيقي إلا بالله"

صدق الله العظيم

DECLARATION

I certify that this thesis submitted for the degree of Master of Physics is the result of may own research, except where otherwise acknowledged, and that this thesis (or any part of the same) has not been submitted for a higher degree to any other university or institution.

Signed: Hazem Salah.

(Hazem Khaleel Wdaa'h Salah)

Date: 4.9.2001

DEDICATION

To My Parents...

And Wife...

With Love...

ACKNOWLEDGMENTS

I would like to express my profound gratitude to my research advisor, Dr. Saker Darwish and the co-advisor Dr. Amin Leghrouz for their guidance and continuous support through all stages of this work. I like to extend my thanks to the faculty and staff at the physics department for their help and support during my graduate work.

Last, but not least, I Thank my Family and Friends for their support and encouragement.

TABLE OF CONTENTS

LIST OF FIGURES

LIST OF TABLES

ABSTRACT

FINE STRUCTURE IN EXCITON-MAGNON BANDS IN Mn^{2+} MAGNETS

This thesis deals with the ${}^6A_{1g}({}^6s) \rightarrow {}^4T_{2g}({}^4D)$ Mn^{2+} transitions in antiferromagnetic $RbMnF_3$ ($T_N = 82.6^\circ K$) compound. Fine structure at low temperature was observed in the D-band of $RbMnF_3$ compound. Tentative assignments of this fine structure are discussed by examining the exchange interaction mechanism, spin wave side bands (i.e. exciton-magnon absorption), vibronic mechanism, and spin-orbit interaction (L-S). The analysis shows that The exchange interaction mechanism plays an important role in the appearance of the fine structure in the D-band. The shift in the line position of the D-band can be quantitatively understood by considering the effect of the exchange interaction between the adjacent Mn^{2+} ions. The disappearance of the fine structure peaks in the D-band above T_N was explained in terms of spin disorder and the lack of exchange interaction between neighboring Mn^{2+} ions. The temperature dependence of the D-band in $RbMnF_3$ above T_N proves that this band is an exciton-magnon band in nature.

CHAPTER I

INTRODUCTION

There are several optical absorption bands in the visible and near-ultra violet region due to crystal-field transitions of the Mn^{2+} ions in type II antiferromagnetic manganese compounds such as $RbMnF_3$ ($T_N = 82.6^{o}K$) and $KMnF_3$ ($T_N = 88.3^{o}K$) [1,2]. The assignments of these bands, namely, A, B, C... represents transitions from the sextet ${}^6A_{1g}$ ground state to the quartet ${}^4T_{1g}(I), {}^4T_{2g}(I), {}^4A_{1g} + {}^4E_g \ldots$ excited states [1,3-5]. These absorptions are due to partially allowed electric dipole $d^5 \rightarrow d^5$ transitions, which are otherwise highly forbidden by spin and parity selection rules. In order to explain how these transitions become allowed and to explain the observed intensities, several papers have discussed the role of exchange and vibronic interactions in making these transitions partially allowed [6-12].

Magnon side bands such as magnon-magnon [12-14], exciton-magnon [9,15-16] and exciton-exciton [17-18,71] have been studied extensively in recent years. The studies of these side bands have provided

a wealth of information about magnons, excitons and have helped to understanding of the role of exchange interaction between magnetic ions. However, most of these studies have been carried out at liquid helium temperatures and mainly concerned with the total bands and with the temperature dependence of the magnon side bands.

Green, Sell, Yen, Shawlow and White first observed Magnon side bands in the absorption spectrum of MnF_2 belonging to the optical transition of ${}^6A_{1g} \rightarrow {}^4T_{1g}$ [15]. Motizuki and Harada [19-20] interpreted theoretically the intensity of exciton-magnon bands in MnO ($T_N = 117^\circ K$) and MnS ($T_N = 147^\circ K$) observed by Huffman [21] using the spin-wave approximations. Tanaka [22] discussed the thermal behavior of magnon side bands for MnF_2 using the Green's function method. Shinagawa and Tanabe [23] derived general expression for the intensity of magnon side bands and gave numerical results for MnF_2 by using the decoupling approximation for correlation functions. Fujiwara and Tanabe [24] carried out numerical calculations for the ${}^6A_{1g} \rightarrow {}^4A_{1g}\,{}^4E_g$ transitions in $RbMnF_3$ and present some theoretical curves for the temperature dependence of the intensity and the line width of the magnon side bands. The line positions shifts with increasing temperatures for magnon side bands in $RbMnF_3$ and

$KMnF_3$ were reported by Ferguson, Guggenheim and Tanabe [5]. But their work was limited to the ${}^6A_{1g} \rightarrow {}^4A_{1g}\,{}^4E$ transitions. Seehra and Abumansoor [25] studied the line positions and line widths of magnon side bands in MnF_2 as a function of temperature in detail. Fine structures in A, C and D bands at low temperatures in MnO were studied by Yokogawa, Taniguchi and Hamaguchi [2]. Exchange interactions between neighboring Mn^{2+} ions and the spin-orbit interaction in $MnBr_2$ were studied in detail by Hoekstra, Folkersma and Haas [26].

Even though many side bands have been identified in different materials [27], the fine structures of only a few side bands have been studied in detail [25]. Therefore the investigation will focus on the fine structure of D-band in $RbMnF_3$ compound at low temperatures, such fine structure have not yet been reported in $RbMnF_3$. In addition the exciton-magnon bands which correspond to the simultaneous creation of an exciton on one magnetic ion and a magnon on the other ion are observed in the D-band.

However, the present work deals with the following aspects:

1) Studying the effect of the crystalline structure on the energy levels of Mn^{2+} ion.

2) Studying the temperature dependence of the line position of D-band, i.e. to look at the behavior of the line position of D-band in $RbMnF_3$ below and above the Neel temperature T_N of this compound.

3) Studying the fine structure of the D-band in $RbMnF_3$.

4) Discussing the role of spin-orbit interaction, exchange interaction and selection rules in making a tentative interpretation of fine structure in the D-band in $RbMnF_3$ compound and in making this transition to be partially allowed.

The proposed thesis is arranged as follows. In chapter II a theoretical Background for crystal field theory, absorption of radiation, selection rules, transition mechanisms, vibronic interaction, exchange interaction are briefly discussed. Chapter III is a review of the experimental results. Chapter IV deals with the theoretical discussion of the experimental results. In chapter V a summary of the major results of this work is given.

CHAPTER II

BACKGROUND AND THEORETICAL CONSIDERATIONS

In this work the energy levels of the manganese ion in a crystal form of $RbMnF_3$ has been studied. This compound is a well-known antiferromagnatic with Neel temperature $T_N = 82.6^{\circ}K$.

To study the energy levels of manganese ion in the crystal form of $RbMnF_3$, one needs to find the electronic energy levels of the Mn^{2+} ion in the host lattice of this compound, and how these energy levels are effected by the crystalline structure. Therefore, we begin with a brief review of the crystal and magnetic structure of this compound, followed by the atomic energy levels of Mn^{2+} as a free ion. And we look at the effect of the octahedral field on the energy levels of Mn^{2+} ion. This is followed by the selection rules governing the absorption of radiation and how these selection rules are affected by vibronic and exchange interaction.

2.1 Crystal structure

$RbMnF_3$ crystallize in the perovskite structure with the space group Pm3m $\left(O_h^1\right)$[28]. The Mn^{2+} ions occupy the corners of a simple cube,

Surrounded by six F^- ions, the $RbMnF_3$ unit cell is shown in figure (2.1). $RbMnF_3$ becomes anti-ferromagnetically ordered below $82.6^{\circ}K$, the lattice parameters and the exchange constants J_1 (nearest neighbor) and J_2 (next nearest neighbor) and Neel temperature T_N are given below [29]:

Lattice constant ($\mathring{A}$)	$T_N(^{\circ}K)$	$J_1(cm^{-1})$	$J_2(cm^{-1})$
a = 4.2396	82.6	2.35	negligible.

$RbMnF_3$ in the antiferromagnetic state has two sublattices of magnetic ions one with spin up and the other with its spin down. $RbMnF_3$ has a solid structure it is known to remain cubic down to liquid helium temperatures.

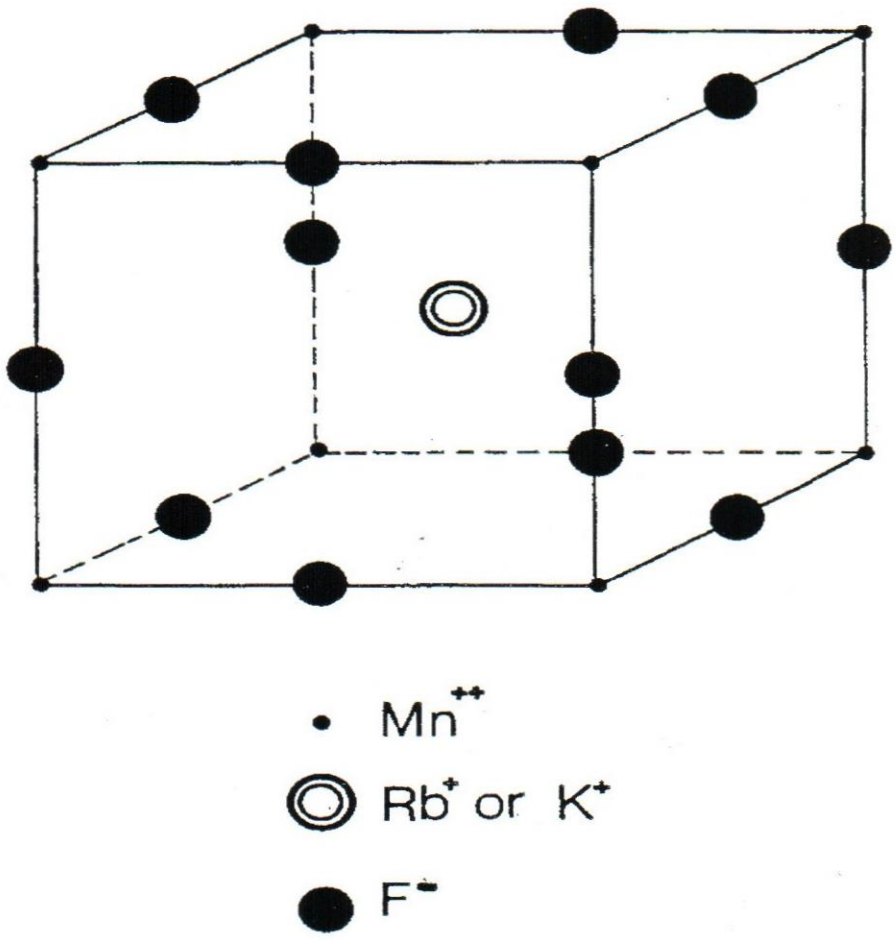

Figure (2.1): The crystal structure of $RbMnF_3$.

2.2 Atomic energy levels of Mn^{2+}

Manganese ion, Mn^{2+}, has the electronic configuration $1S^2 2S^2 2P^6 3S^2 3P^6 3d^5$. To obtain the ground state, one follows hund's rules which yield a ${}^6S$ (sextet) state for the ground state for the $3d^5$ configuration. Some possible excited states are ${}^4G, {}^4P, {}^4D, {}^4F, etc.$ [30].

The actual calculation of the energy levels of the Mn^{2+} free ion was done by Slater and Condon [3] in terms of their parameters $F_0, F_2,$ and F_4, and these parameters are outlined in appendix (A) [31]. Table (2.1) shows the theoretical energies of sextet and quartet terms for the $3d^5$ configuration [32]. The relations between Slater-Condon parameters and the well-known Racah parameters [33] A, B, and C are given as follows:

$$A = F_o - 49\ F_4$$

$$B = F_2 - 5\ F_4$$

$$C = 35\ F_4$$

The values of Racah parameters in (cm^{-1}) are usually determined by the best fit to experimental results. As an example, for $RbMnF_3$, the Racah parameters are given as B = 700 cm^{-1}, C = 3650 cm^{-1}. Another parameter is the crystal field parameter Dq (discussed later) which equals 750 cm^{-1} in $RbMnF_3$ [3].

Table (2.1)

Theoretical Energies of Sextet and Quartet

Terms for the ($3d^5$) configuration.

Terms	Slater-Condon Parameters	Racah Parameters
^6S	$10\,F_o - 35\,F_2 - 315\,F_4$	$10\,A - 35\,B$
^4G	$10\,F_o - 25\,F_2 - 190\,F_4$	$10\,A - 25\,B + 5\,C$
^4F	$10\,F_o - 13\,F_2 - 180\,F_4$	$10\,A - 13\,B + 7\,C$
^4D	$10\,F_o - 18\,F_2 - 225\,F_4$	$10\,A - 18\,B + 5\,C$
^4P	$10\,F_o - 28\,F_2 - 105\,F_4$	$10\,A - 28\,B + 7\,C$

In the free ion, the d electrons may occupy the five-d orbital with equal energies. The wave functions are given by:

$$\Psi_{n,l,m_l} = R_{n,l} \quad Y_l^{m_l},$$

Where (n) is the principle quantum number, (l) is the orbital quantum number, and (m_l) is the quantum number specifying the component of this angular momentum in the Z-direction. Also, (R_{nl}) is the radial part of the wave function, and ($Y_l^{m_l}$) is the spherical harmonic. The angular dependence of the d orbital with ($l = 2$) is given by [34]:

$$Y_2^0 = (5/8)^{1/2}(3\cos^2\theta - 1)(2\pi)^{-1/2}$$

$$Y_2^{\pm 1} = (15/4)^{1/2}\sin\theta\cos\theta\ (2\pi)^{-1/2} e^{\pm i\phi}$$

$$Y_2^{\pm 2} = (15/16)^{1/2}\sin^2\theta\ \ (2\pi)^{-1/2} e^{\pm 2i\phi}.$$

The five wave functions in their real forms are obtained by taken the suitable combinations of the above spherical harmonics. The d orbital functions are expressed as follows:

$$d_{z^2} = (Y_2^0)$$

$$d_{yz} = \frac{1}{\sqrt{2}}\left[(Y_2^{+1}) - (Y_2^{-1})\right]$$

$$d_{xz} = \frac{1}{\sqrt{2}}\left[(Y_2^{+1}) + (Y_2^{-1})\right]$$

$$d_{xy} = \frac{1}{\sqrt{2}}\left[(Y_2^{+2}) - (Y_2^{-2})\right]$$

$$d_{x^2-y^2} = \frac{1}{\sqrt{2}}\left[(Y_2^{+2}) + (Y_2^{-2})\right]$$

2.3 Crystal Field Theory

Crystal field theory treats the effects of the electric field due to the presence of the neighboring ions called ligands, on the central ion [34].

Taking the $RbMnF_3$ compound, and by using the point charge model. The manganese ion is the ion of interest and it is surrounded by six F^-, called ligands. These ligands create an electric field, which destroy the spherical symmetry of the manganese ion. The ligands are taken to be points of negative charges, and the metal ions are considered to be non-interacting ions [35].

The theory of crystal field has been studied in many books, e.g. by Ballhausen [36], Griffith [37], and Low [38]. The basic idea is to treat the potential due to the ligands as a perturbation to the Hamiltonian of the free

two perturbing terms, the electronic repulsion term and the spin-orbit term. Therefore it is necessary to distinguish three cases:

i) Weak crystal field: $\sum_{ij} \lambda_{ij} L_i . S_j < V_C \leq \sum_{i \neq j} \frac{e^2}{r_{ij}}$

ii) Medium crystal field: $V_C < \sum_{ij} \lambda_{ij} L_i . S_j < \sum_{i \neq j} \frac{e^2}{r_{ij}}$

iii) Strong crystal field: $V_C \geq \sum_{i \neq j} \frac{e^2}{r_{ij}} > \sum_{ij} \lambda_{ij} L_i . S_j$

In reality there is no separation between one case and the other, but the relative order of magnitude is very important to decide at what point in the calculation the crystalline field will be used as perturbation.

There are two well-known approaches which are used to make a calculation for the effect of the crystal field on the energy states of the central ion, they are:

1) The weak field scheme, where the coulomb interaction between electrons is considered first in determining the energy levels of the free ion, and the ligands field is considered to cause new change in the energy levels. Orgel's calculation is based on this approach [39].

2) The strong field scheme, which takes into account a crystal field first, followed by the coulomb interaction. This scheme was developed by Tanabe and Sugano [40]. Both approaches are considered to be successful leading to the same results. Spin-orbital interaction is small and treated as a perturbation [41].

2.4 Octahedral Fields

In order to evaluate the effect at the crystal field potential on the energy levels of the central ion, one must determine the potential due to these negative charges at a general point inside the octahedron (Fig.B.1). This is a standard problem in classical electrostatics [42-44], and is briefly outlined in Appendix (B).

The potential due to a cubic field is given by:

$$V_C = \frac{6Ze^2}{a} + D\left[x^4 + y^4 + z^4 - \frac{3}{5}r^4\right] \qquad (2.4.1)$$

where $D = \frac{35Ze^2}{4a^5}$. The term $\frac{6Ze^2}{a}$ is clearly spherically symmetrical and cannot cause splitting of the levels. All it does is to raise the whole set of d - orbital energies by the same amount. Therefore this term can be ignored

in determining a splitting of the energy levels. In terms of spherical harmonics, the remaining potential is expressed as:

$$V_C = \frac{7Ze^2}{3a^5}\sqrt{\pi}\, r^4\left[Y_4^0 + \sqrt{\frac{5}{14}}(Y_4^4 + Y_4^{-4})\right] \qquad (2.4.2)$$

Considering V_C as a perturbation in the Hamiltonian, and by using the perturbation theory, the first-order energy will be:

$$<\Psi \mid V_C \mid \Psi> = \int \Psi^* V_C \Psi \, d\tau \qquad (2.4.3)$$

Where Ψ is the atomic wave function for d state.

The effect of the octahedral field is easily demonstrated by considering the d^1 configuration. The wave function is:

$$\Psi_{n,l,m_l} = R_{n,l}(r)\ \Theta_{l,m_l}(\theta)\ \Phi_{m_l}(\phi)$$

And the matrix elements of V_C between the states with quantum numbers (nlm_l) and $(nl'm_l')$ may be written as:

$$\begin{aligned}&\int_0^{\infty}\int_0^{\pi}\int_0^{2\pi} R_{n,l}(r)\Theta_{l,m_l}(\theta)\Phi_{m_l}(\phi)V_C R_{n,l'}(r)\Theta_{l',m_{l'}}(\theta)\Phi_{m_{l'}}(\phi)r^2\sin\theta dr d\theta d\phi \\ &= \langle R_{n,l}|V(r)|R_{n,l}\rangle\langle lm_l|V(\theta,\phi)|l'm_{l'}\rangle\end{aligned} \qquad (2.4.4)$$

Since m_l has $(2l+1) = 5$ values (i.e. $-2 \le m_l \le 2$) for the d state, then we expected to have a 5×5 secular determinant. The Θ and Φ integrals may be evaluated but the radial part can not be done because it is necessary to specify which set of d electrons is being dealt with, and is therefore replaced by a parameter [45]. For example,

$$\frac{2}{105}\int_0^{\infty} R^*_{n,l}(r)\ r^4\ R_{n,l}(r)\, r^2 dr = q \qquad (2.4.5)$$

Evaluations for the non-vanishing matrix elements are shown in Appendix (C), and the results are:

$$\begin{aligned} &< 2 \mid V_C \mid 2 > = < -2 \mid V_C \mid -2 > = Dq \\ &< -2 \mid V_C \mid 2 > = < 2 \mid V_C \mid -2 > = 5Dq \\ &< 1 \mid V_C \mid 1 > = < -1 \mid V_C \mid -1 > = -4Dq \\ &< 0 \mid V_C \mid 0 > = 6Dq \end{aligned} \qquad (2.4.6)$$

And the secular determinant becomes:

$$\begin{array}{ccccc} (2) & (1) & (0) & (-1) & (-2) \\ \left|\begin{array}{ccccc} Dq - E & 0 & 0 & 0 & 5Dq \\ 0 & -4Dq - E & 0 & 0 & 0 \\ 0 & 0 & 6Dq - E & 0 & 0 \\ 0 & 0 & 0 & -4Dq - E & 0 \\ 5Dq & 0 & 0 & 0 & Dq - E \end{array}\right| & = 0 \end{array} \qquad (2.4.7)$$

This determinant may immediately be reduced to the sub determinants as follows:

$$\begin{array}{cc} (1) & (-1) \\ \left|\begin{array}{cc} -4Dq - E & 0 \\ 0 & -4Dq - E \end{array}\right| & = 0 \end{array} \qquad (2.4.8.a)$$

$$\begin{array}{c} (0) \\ \left|\begin{array}{c} 6Dq - E \end{array}\right| = 0 \end{array} \qquad (2.4.8.b)$$

These determinants are readily solved to yield the following roots:

$$E = -4Dq,\ E = -4Dq \text{ and } E = 6Dq.$$

and the determinant:

$$\begin{array}{cc} (2) & (-2) \\ \left| \begin{array}{cc} Dq - E & 5Dq \\ 5Dq & Dq - E \end{array} \right| & = 0 \end{array} \qquad (2.4.8.c)$$

This last determinant is readily solved to yield the energies -4Dq and 6Dq. Therefore, the roots of the determinant in Eq. (2.4.7) are:

$$E_e = 6Dq \quad \text{(Doublet)}.$$

$$E_t = -4Dq \quad \text{(Triplet)}. \qquad (2.4.9)$$

The five-fold degeneracy has been removed and replaced by two new levels. The upper level is doubly degenerate, and the lower is triply degenerate and they are separated by 10Dq as shown in figure (2.2).

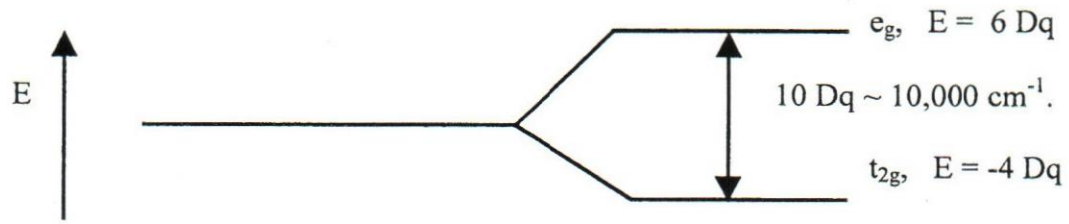

$$\Delta E = (6Dq) - (-4Dq) = 10Dq.$$

Figure (2.2): Splitting of the d orbitals in an octahedral field.

The wave functions for the ion are determined by substituting for the energies in the secular determinant and the results are [46]:

$$\begin{aligned}
e_g: \quad & d_{x^2-y^2} = \frac{1}{\sqrt{2}}(d_2 + d_{-2}) = \frac{\sqrt{3}}{2}(x^2 - y^2) \\
& d_{z^2} = d_0 = \frac{1}{2}(3z^2 - r^2) \\
& d_{xy} = \frac{1}{i\sqrt{2}}(d_2 - d_{-2}) = \sqrt{3}(xy) \\
t_{2g}: \quad & d_{xz} = -\frac{1}{\sqrt{2}}(d_1 - d_{-1}) = \sqrt{3}(xz) \\
& d_{yz} = -\frac{1}{i\sqrt{2}}(d_1 + d_{-1}) = \sqrt{3}(yz)
\end{aligned} \tag{2.4.10}$$

Note that the densities of e_g electrons are directed toward the ligands (i.e. negative charges), whereas those of the t_{2g} electrons avoid these regions as

shown in the figure (2.3). It is clear that an electron in the d orbitals will favor the t_{2g} orbitals to avoid repulsion from the ligand atoms. For the Mn^{2+} (d^5) configuration, the method for obtaining the energy levels under the influence of the octahedral field potential was discussed, and the actual perturbation secular determinants were obtained by Orgel [47], Tanabe and Sugano [48], and Low [49].

The effect of the octahedral field on the energy levels of the free ion may be seen from figure (2.4). For the ground state we have an ${}^6S$ term which is orbitally non-degenerate. Since the ligand's field potential is concerned only with the orbital part of a wave function, it cannot split an S term. For the P level, even though it is orbitally degenerate, all matrix elements for the octahedral field potential vanish and therefore the P level does not split. Under the orthorhombic symmetry, the P level splits into three levels. For the other levels there are further splittings, because all of the levels are orbitally degenerate and have non-vanishing matrix for the octahedral potential. As an example, the ${}^4G$ level has a degeneracy of nine. Under octahedral symmetry it splits to ${}^4A_{1g}, {}^4E_g, {}^4T_{1g}, and {}^4T_{2g}$. The E and T levels may split further under the effect of lower symmetry. Also, the total behavior of the levels with the increased Dq is shown in the Orgel [50] diagram in figure (2.5).

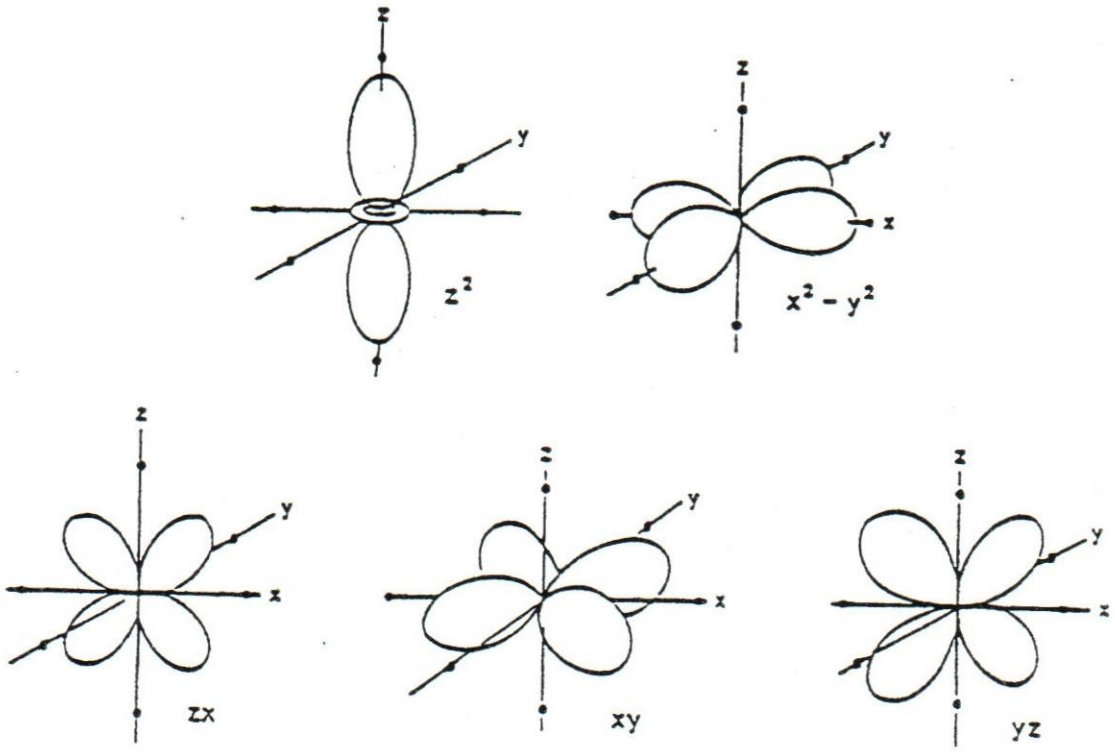

Figure (2.3): Angular parts of d wave function in a cubic crystal [Ref. 32].

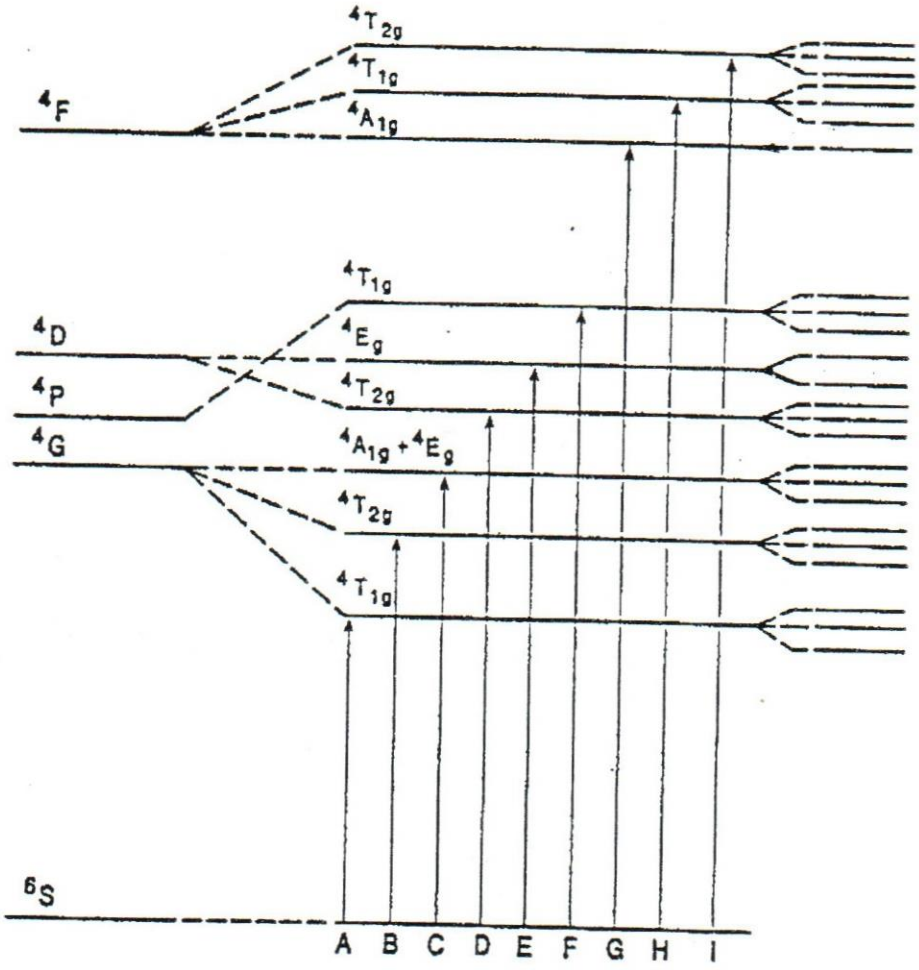

Figure (2.4): Schematic diagram showing the electronic energy levels of the Mn^{2+} ion in the cubic crystal field potential.

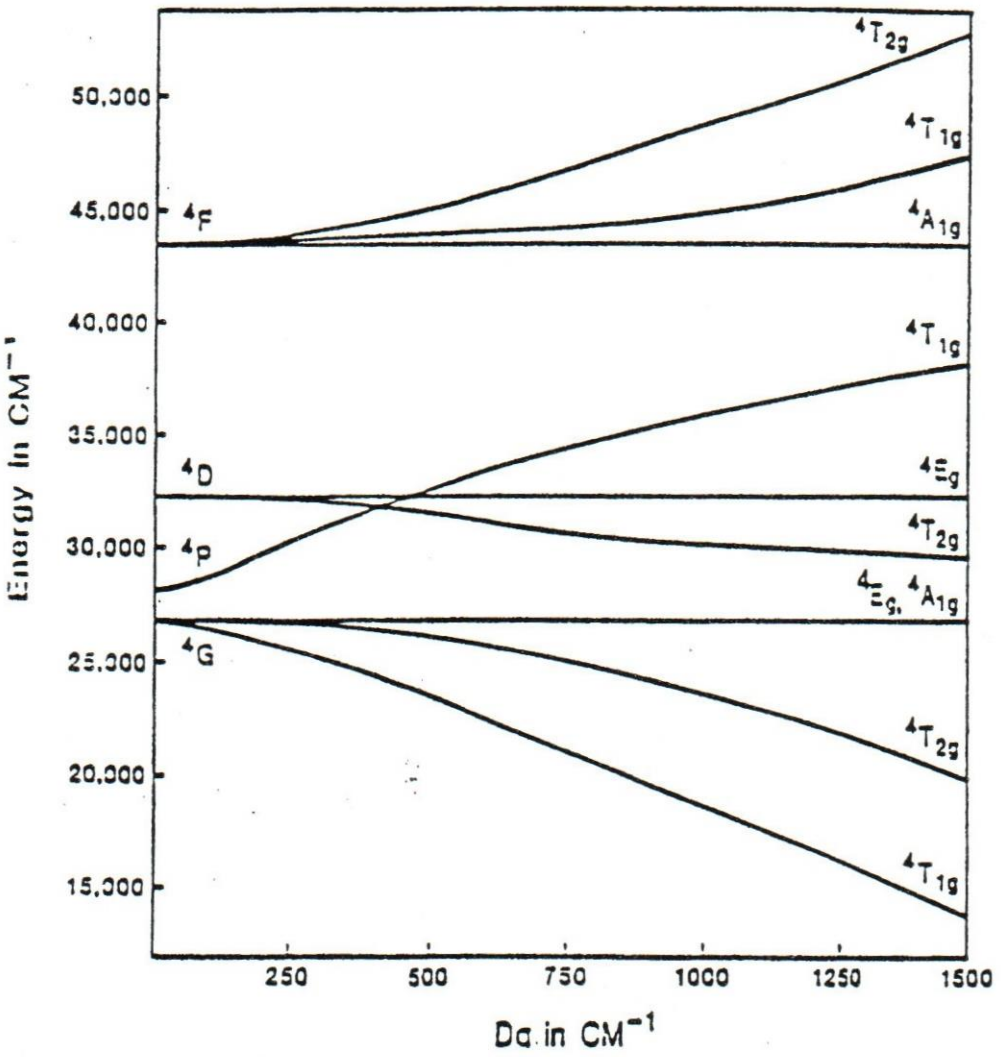

Figure (2.5): Orgel digram showing the splitting of the $3d^5$ terms by the crystal field of O_h symmetry and their variation as a function of Dq [Ref.50].

2.5 Absorption of Radiation.

To study how the absorption of radiant energy causes the system to go from one state to another state. We need to take into account the changes to the original Hamiltonian, when the electromagnetic radiation falls on the system. The electric field of the incident radiation may interact with the system adding a perturbation term to the original Hamiltonian. The Hamiltonian may be written in the form given below:

$$H = \frac{1}{2m}\left(\vec{P} - \frac{e}{c}\vec{A}\right)^2 + e\phi \qquad (2.5.1)$$

where $\vec{P}$ is the momentum, $\vec{A}$ is the vector potential, and ϕ is the electrostatic scalar potential. The operators $\vec{P}$ and $\vec{A}$ do commute whenever the vector potential field $\vec{A}$, is constant in time [51] and the Hamiltonian then becomes:

$$H = \frac{P^2}{2m} + e\phi - \frac{e}{mc}\vec{P}.\vec{A} + \frac{e^2}{2mc^2}A^2. \qquad (2.5.2)$$

The second-order term will contribute to the transition with the emission of two photons, but it will not contribute to the transition accompanied by the emission or absorption of a single photon. The probability for a transition involving two photons involves a factor α^2, $(\alpha^2 = (\frac{e^2}{\hbar c})^2 \cong (\frac{1}{137})^2)$, whereas

the one-photon transition probability is proportional to α. Therefore, the second-order term may be ignored compared to the first-order term and we are left with $-\frac{e}{mc}\vec{P}.\vec{A}$ as the leading perturbation term [52]. The vector potential $\vec{A}$ may be expressed as the real part of a plane wave,

$$\vec{A} = \overrightarrow{A_o} e^{i(\vec{k}.\vec{r}-wt)} \tag{2.5.3}$$

where r is the radius of the atom ($\approx \overset{o}{\text{A}}$), and the wave length in the visible range is between $(3000 - 6000)\ \overset{o}{\text{A}}$. Therefor, $\vec{k}.\vec{r} << 1$, and the exponential may be expanded in a power series as follows:

$$\vec{A} = \overrightarrow{A_o} e^{-iwt}\left[1 + (i\vec{k}.\vec{r}) + \frac{(i\vec{k}.\vec{r})^2}{2} + - - - - - - - \right] \tag{2.5.4}$$

Considering the first term and following Anderson [53], the perturbation is

$$\frac{e}{mc}\vec{P}.\overrightarrow{A_o} \tag{2.5.5}$$

If the plane wave is polarized in the x-direction then

$$\vec{P}.\overrightarrow{A_o} = P_x A_o$$

and the matrix element of the perturbation between states j and k is:

$$H^1_{kj} = \frac{eA_o}{2mc}\langle k|P_x|j\rangle \tag{2.5.6}$$

and using $P_x = m\dot{x} = \frac{im}{\hbar}[H_o, x]$, then Eq. (2.5.6) becomes:

$$H^1_{kj} = \frac{ieA_o}{2c\hbar}\left[\langle k|H_o x|j\rangle - \langle k|xH_o|j\rangle\right] \tag{2.5.7}$$

$$= \frac{ieA_o}{2c\hbar}\left[\langle H_o k|x|j\rangle - \langle k|x|H_o j\rangle\right]$$
$$= \frac{ieA_o}{2c\hbar}\left(E^o_k - E^o_j\right)\langle k|x|j\rangle$$
$$= \frac{iA_o v\pi}{c}\langle k|ex|j\rangle$$

$$= \frac{iA_o v\pi}{c}\langle D_x\rangle_{kj} \tag{2.5.8}$$

where $(D_x = ex)$is the dipole moment and $(v)$is the frequency of the absorbed photon. For this reason such a transition is called an electric dipole transition. If we take the second-term of the expansion in Eq. (2.5.4), this will introduce an additional factor of:

$$\left(i\vec{k}.\vec{r}\right)\left(\vec{A_o}.\vec{P}\right)$$

and produce components of a second rank tensor [54] corresponding to magnetic dipole moments and electric quadrupole moments. The transition rate from the initial state j to final state k is given by Fermi's golden rule No.2 [55].

$$I = \frac{2\pi}{\hbar}\left|H^1_{kj}\right|^2 \rho(E)_k\,\delta\left(E_{kj} \pm E\right) \tag{2.5.9}$$

where $E = \hbar w$ is the photon energy. From this expression it is clear that transitions can occur only if the matrix element does not vanish.

There are primarily three kinds of transitions that can take place between allowed energy levels with the absorption or emission of electromagnetic radiation. These are:

i) Electric dipole transition.

ii) Magnetic dipole transition.

iii) Electric quadrupole transition.

For the electric dipole transition it has been justified that taking the first term of Eq. (2.5.4) is a good approximation. Therefore to have an electric dipole transition, the parity of the initial and final states must be different. The magnetic and electric quadrupole transitions are the results of considering the next term of the expansion in Eq. (2.5.4) as shown explicitly by Griffith [56]. The probability of these two transitions relative to the electric dipole transition is very small.

2.6 Selection Rules

All the possible transitions as stated previously are governed by certain selection rules. These selection rules are determined by the non-vanishing of the matrix elements in the Fermi's golden rule.

For the electric dipole transitions the matrix elements of the components of the dipole moment operator may be written using the hydrogen like state as [57]:

$$\langle \psi' | D_x | \psi \rangle = \langle \psi' | e.x | \psi \rangle$$

but $\vec{r} = xi + yj + zk = (r\sin\theta\cos\phi)i + (r\sin\theta\sin\phi)j + (r\cos\theta)k$

Therefore: $\langle \psi' | D_x | \psi \rangle = \langle \psi' | er\sin\theta\cos\phi | \psi \rangle$

$$= e\langle n' | r | n \rangle \langle l' | \sin\theta | l \rangle \langle m' | \cos\phi | m \rangle$$

$$\langle \psi' | D_x | \psi \rangle = e\langle n' | r | n \rangle \delta_{l',l\pm1} \delta_{m',m\pm1}$$

$$\langle \psi' | D_z | \psi \rangle = e\langle n' | r | n \rangle \delta_{l',l\pm1} \delta_{m',m} \quad \langle \psi' | D_y | \psi \rangle = e\langle n' | r | n \rangle \delta_{l',l\pm1} \delta_{m',m\pm1}.$$

This leads to the following selection rules for the electric dipole transition:

$$\Delta l = l' - l = \pm 1$$
$$\Delta m = m' - m = 0, \pm 1$$

Since the electric dipole operator does not act on the spin, hence the spin cannot flip in the transition. This leads to the additional selection rule:

$$\Delta S = 0$$

which means that both states must have the same spin quantum number.

Since we are dealing with manganese compounds which have d^5 configuration. The electric transitions between the d^n levels are forbidden. The d^n levels wave functions are symmetric under inversion [58], and the dipole moment operator $\vec{er}$ is odd. Therefor the whole integral is odd between symmetric limits and vanishes. Also the spin of the sextet (ground) states is different from the quartet (excited) states (i.e. $\Delta s \neq 0$). It can be determined which transitions are allowed and which are not by using the point group character table for O_h symmetry. From Table (2.2) the direct product of the ground and the excited state symmetries must transform like T_{1u} to have an allowed electric dipole transition. Since all the resultant states from the crystal field effect are gerade (g), then the transitions are symmetry forbidden. According to Laporte's Rule: Only transitions between an even state and an odd state are allowed as electric dipole transitions.

For the magnetic dipole transitions, the transition probabilities between levels that have quantum number m_j depend upon the existence of a non-vanishing matrix element of the form $\langle \psi' | \vec{L} + 2\vec{S} | \psi \rangle$. For the d^5 levels $\langle \psi' | \vec{L} | \psi \rangle$ does not vanish, because $\vec{L}$ transforms as T_{1g} (even), and using the multiplication table (2.2) shows that transitions are allowed. The matrix element for the spin part $\langle \psi' | 2\vec{S} | \psi \rangle$ will vanish for transitions from the ground state to the excited states in d^5 compounds because these states differ in their spin quantum number S. However, the spin transition may be allowed when the spin-orbit interaction is considered. For magnetic dipole transitions the selection rules are [59]:

$$\Delta j = 0; \Delta m_j = 0, \pm 1; \text{ No parity change.}$$

For the electric quadrupole transitions the selection rules are [60]:

$$\Delta j = 0, \pm 1, \pm 2; \Delta m_j = 0, \pm 1, \pm 2; \text{No parity change.}$$

These transitions are allowed for d^n levels, but their intensities are much less than those for the magnetic dipole transition, and therefore they are difficult to verify experimentally.

2.7 Vibronic Interaction.

From the selection rules we can see that electric dipole transitions are forbidden in the manganese ion. A possible explanation to overcome parity selection rule and partially allows these transitions is to take into account the fact that the ligand atoms of a complex do vibrate, and a suitable combination of the vibrations in the ground and excited electronic states could destroy the center of symmetry which relaxes parity selection rule [61].

To understand this let us suppose that Q represents an odd vibrational coordinate. Then the crystalline field potential may be expanded as:

$$V = V_0 + Q\frac{\partial V}{\partial Q} + \text{----------} \tag{2.7.1}$$

Since V has to remain totally symmetric, both Q and $\frac{\partial V}{\partial Q}$ should have odd symmetry. Then based on Ballhausen's argument, we can mix some odd functions into our even functions, by using the first order perturbation theory [62]:

$$\psi = \psi_g - \frac{Q\int \psi_g \frac{\partial V}{\partial Q}\psi_u}{(E_u - E_g)}\psi_u \tag{2.7.2}$$

where ψ_g represents the unperturbed even wave function and ψ_u is an excited state of odd wave function. For simplicity the initial and final states can be written as:

$$\psi_i = \psi_g + Q\lambda\psi_u$$

$$\psi_f = \psi_g' + Q\lambda'\psi_u' \tag{2.7.3}$$

where λ and λ' denotes the values of the integral for initial and final states respectively. Let χ_p and χ_q to be the vibrational wave functions represented by the harmonic oscillator functions with quantum numbers p and q, respectively. Then the vibronic wave function may be represented as:

$$\psi_{ip} = (\psi_g + Q\lambda\psi_u)\chi_p = \psi_i\chi_p$$

$$\psi_{fq} = (\psi_g' + Q\lambda'\psi_u')\chi_q = \psi_f\chi_q \tag{2.7.4}$$

The probability of a transition from the initial state to final state is proportional to:

$$\left|R_{ip,fq}\right|^2 = \left|\iint \psi_{ip}^* er\psi_{fq} d\tau_{elect} d\tau_{vib}\right|^2 = \left|\left\langle \psi_{ip}\left|\vec{er}\right|\psi_{fq}\right\rangle\right|^2 \tag{2.7.5}$$

where $\vec{er}$ is the electric dipole operator. Substituting Eq. (2.7.4) into Eq. (2.7.5) and dropping the non-contributing matrix elements will give:

$$R_{ip,fq} = \langle \psi_{ip} | \vec{er} | \psi_{fq} \rangle = \int [\lambda' \psi_g^* . \vec{er} \psi_u' + \lambda \psi_u^* . \vec{er} \psi_g'] d\tau_{elec.} \int \chi_p^* Q \chi_q d\tau_{vib.}$$

$$\langle \psi_{ip} | \vec{er} | \psi_{fq} \rangle = [\lambda' \langle \psi_g | \vec{er} | \psi_u' \rangle + \lambda \langle \psi_u | \vec{er} | \psi_g' \rangle] . \langle \chi_p | Q | \chi_q \rangle \qquad (2.7.6)$$

From Eq. (2.7.6) we can see that transitions are allowed only if the vibrational states p and q differ by one quantum. Also it may be noted that the intensity is proportional to the value of the vibrational matrix, which in turns is proportional to the square root of p and q, whichever is the greater [63]. At higher temperatures, the stronger bands appear, corresponding to larger amplitudes of vibration and greater distortions. For example, the band intensity is proportional to:

$$\coth(h\nu/2kT) .$$

Relaxation of the parity selection rule may be also explained using Multiplication tables in group theory. The idea is based on Cotton's [64] and Figgis's [34] arguments, which involves the use of the combination of electronic and vibrational wave functions to represent the ground and the excited states. The symmetry representation of these states can be found by

taking the direct product of the representations of $\psi_{\text{electronic}}$ and $\psi_{\text{vibration}}$. In general most complexes have several vibrational modes available to the ground and excited states, then it is most likely that for a certain mixing between ground state and excited state the transition becomes slightly allowed.

If we examine an octahedral complex where the manganese ion is at the center of symmetry, then the normal modes of vibrations are:

$$A_{1g}, E_g, T_{1u}, T_{2g}, T_{2u}$$

where T_{1u} and T_{2u} are the symmetries of the odd vibration as shown in figure (2.6) [65].

If we consider the pure electronic transition ${}^1A_{1g} \rightarrow {}^1T_{2g}$, then by using the multiplication table (2.2), the direct product in the group O_h,

$$\Gamma({}^1A_{1g} \left| \vec{er} \right| {}^1T_{2g}) = T_{2g} x T_{1u} x A_{1g} \qquad (2.7.7)$$

$$= T_{2g} x T_{1u}$$

$$= T_{1u} + T_{2u} + E_u + A_{2u}$$

does not contain A_{1g}. Consequently, the transition is not allowed, but if there are simultaneous excitation of a vibration of T_{1u} or T_{2u} symmetry, then after the multiplication we have:

$$T_{1u} x T_{1u} x A_{1g} = T_{1u} x T_{1u} = A_{1g} + E_g + T_{1g} + T_{2g}.$$

which contains A_{1g} and the transition is allowed. Take another example, the $^1A_{1g} \rightarrow {}^1T_{1g}$ transition, the direct product give:

$$\Gamma(^1A_{1g} \left| \vec{er} \right| {}^1T_{1g}) = T_{1g} x T_{1u} x A_{1g}$$

$$= T_{1g} x T_{1u}$$

$$= A_{2u} + E_u + T_{1u} + T_{2u}.$$

None of these contain A_{1g}, but it becomes allowed with the simultaneous excitation of T_{1u} and T_{2u} vibrations i.e.,

$$T_{1u} x T_{1u} x A_{1g} = T_{1u} x T_{1u} = A_{1g} + E_g + T_{1g} + T_{2g}.$$

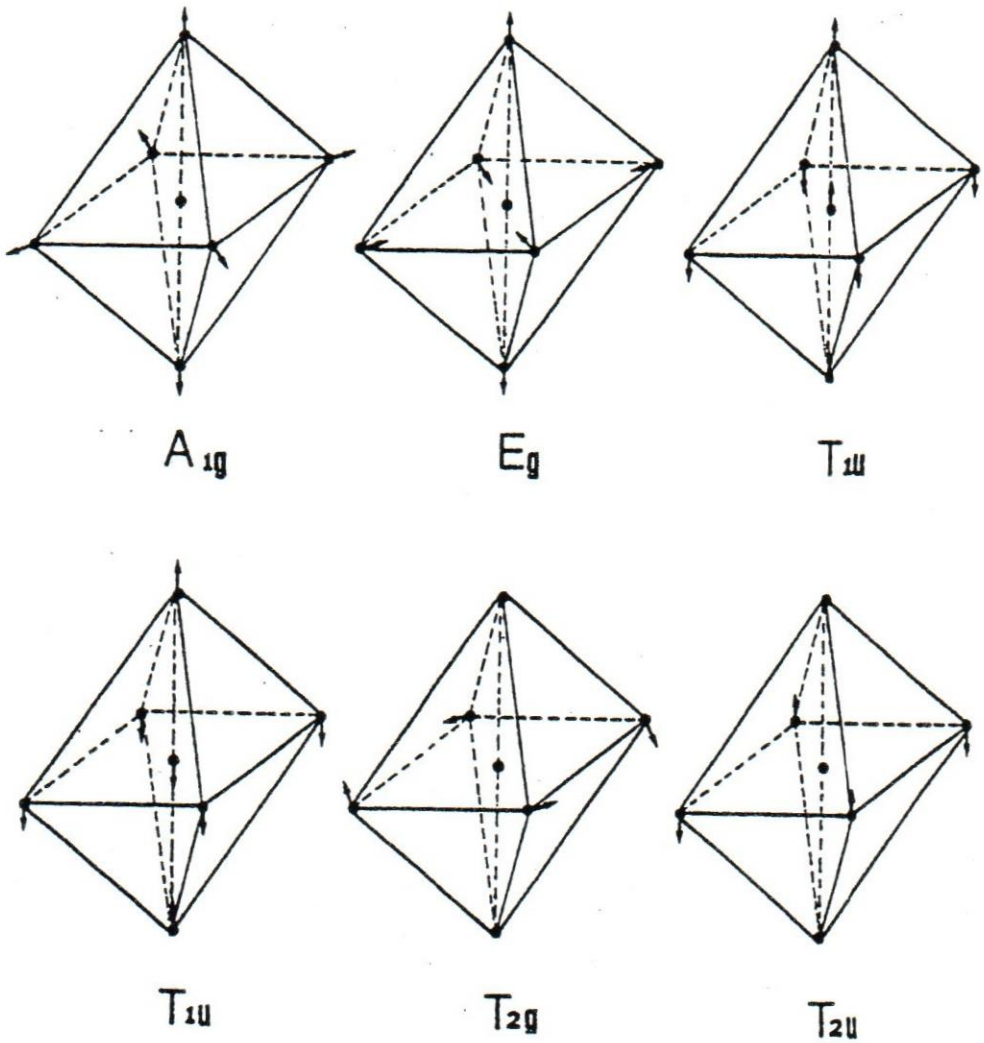

Figure (2.6): Normal vibrations of an octahedral point group O_h [Ref.65].

Table (2.2)

Multiplication Table for O_h Group.

	A_{1g}	A_{2g}	E_g	T_{1g}	T_{2g}	A_{1u}	A_{2u}	E_u	T_{1u}	T_{2u}
A_{1g}	A_{1g}									
A_{2g}	A_{2g}	A_{1g}								
E_g	E_g	E_g	$A_{1g}+A_{2g}+E_g$							
T_{1g}	T_{1g}	T_{2g}	$T_{1g}+T_{2g}$	$A_{1g}+E_g+T_{1g}+T_{2g}$						
T_{2g}	T_{2g}	T_{1g}	$T_{1g}+T_{2g}$	$A_{2g}+E_g+T_{1g}+T_{2g}$	$A_{1g}+E_g+T_{1g}+T_{2g}$					
A_{1u}	A_{1u}	A_{2u}	E_u	T_{1u}	T_{2u}	A_{1g}				
A_{2u}	A_{2u}	A_{1u}	E_u	T_{2u}	T_{1u}	A_{2g}	A_{1g}			
E_u	E_u	E_u	$A_{1u}+A_{2u}+E_u$	$T_{1u}+T_{2u}$	$T_{1u}+T_{2u}$	E_g	E_g	$A_{1g}+A_{2g}+E_g$		
T_{1u}	T_{1u}	T_{2u}	$T_{1u}+T_{2u}$	$A_{1u}+E_u+T_{1u}+T_{2u}$	$A_{2u}+E_u+T_{1u}+T_{2u}$	T_{1g}	T_{2g}	$T_{1g}+T_{2g}$	$A_{1g}+E_g+T_{1g}+T_{2g}$	
T_{2u}	T_{2u}	T_{1u}	$T_{1u}+T_{2u}$	$A_{2u}+E_u+T_{1u}+T_{2u}$	$A_{1u}+E_u+T_{1u}+T_{2u}$	T_{2g}	T_{1g}	$T_{1g}+T_{2g}$	$A_{2g}+E_g+T_{1g}+T_{2g}$	$A_{1g}+E_g+T_{1g}+T_{2g}$

2.8 Exchange Interaction.

To explain the difference in intensities of the absorption bands between one manganese compound and another, I need to consider a mechanism that relaxes the spin selection rules. The idea is to consider that there is an interaction between a pair of ions in magnetic crystals. This idea was introduced by Tanabe, Moriya and Sugano [66]. They suggested that the effective spin-dependent electric dipole moment between two ions has the form:

$$\overrightarrow{P_{eff}} = \Pi_{ij}(\overrightarrow{S_i}.\overrightarrow{S_j}) \qquad (2.8.1)$$

where S_i and S_j are the spin operators, i and j refer to electrons on the spin - down and spin-up sublattices, Π is the transition dipole moment. Expressions for the Π_{ij} were obtained by Tanabe and Gondaira [67].

There are three forms of transitions results when we applying the exchange interaction mechanism. They are:

i) Two-magnon transitions.

ii) Exciton-magnon transitions.

iii) Two-exciton transitions.

These transitions stated above are shown in figure (2.7) and have been confirmed experimentally [68-71].

To understand how these transitions can take place, let us take the exciton-magnon transition as an example. A simple diagram as shown in figure (2.8.a) may represent this transition. Initially both ions are in the ground states, as a result of absorbing a photon they end up with final states of an exciton for one ion and magnon for the other. In this case the Hamiltonian of the crystal can be written as [68]:

$$H = H_0 + V + \vec{\varepsilon}.\vec{P} \tag{2.8.2}$$

where H_0 is the sum of all single-ion Hamiltonians, V is the sum of all two-ion interactions, $\vec{\varepsilon}$ is the electric field and $\vec{P}$ is the sum of the electric-dipole operator of all electrons.

To make a connection between initial and final states (Fig. 2.8.a) a second order process that including nondiagonal exchange connects the initial and final states via an intermediate state and this can be written as [68]:

$$\langle F|H_{eff}|G\rangle = \sum_u \varepsilon \left[\frac{< F|V|U >< U|P|G >}{(E_G - E_U + h\nu)} + \frac{< F|P|U' >< U'|V|G >}{(E_G - E_{U'})} \right] \tag{2.8.3}$$

here $|F\rangle$ is the final exciton-magnon state, $|U\rangle$ and $|U'\rangle$ are an intermediate states of opposite parities (odd states) to the ground states (even states) to overcome the parity selection rule, $|G\rangle$ is the ground state, E_G and E_U are the energies for states G and U, respectively. $h\nu$ is the energy of the absorbed photon, and H_{eff} is the effective Hamiltonian combining V and P, and the sum is taken over all intermediate states.

To study Eq. (2.8.3), we need to examine each term with the aid of figure (2.8). Let us first take $\langle U|P|G\rangle$ term, which may be written as:

$$\langle U|P|G\rangle = \langle u_{01}|p_{01}|g_{01}\rangle \tag{2.8.4}$$

This make a connection between the ground state g_{01} (the number 0 represents the reference ion and number 1 refers to the up-sublattice) and the intermediate odd state u_{01} (for the reference ion on sublattice 1) at the same sublattice with $M_s = 5/2$ spin state. Since this take place on the same sublattice we have $\Delta S = 0$ as indicated in figure (2.8.b).

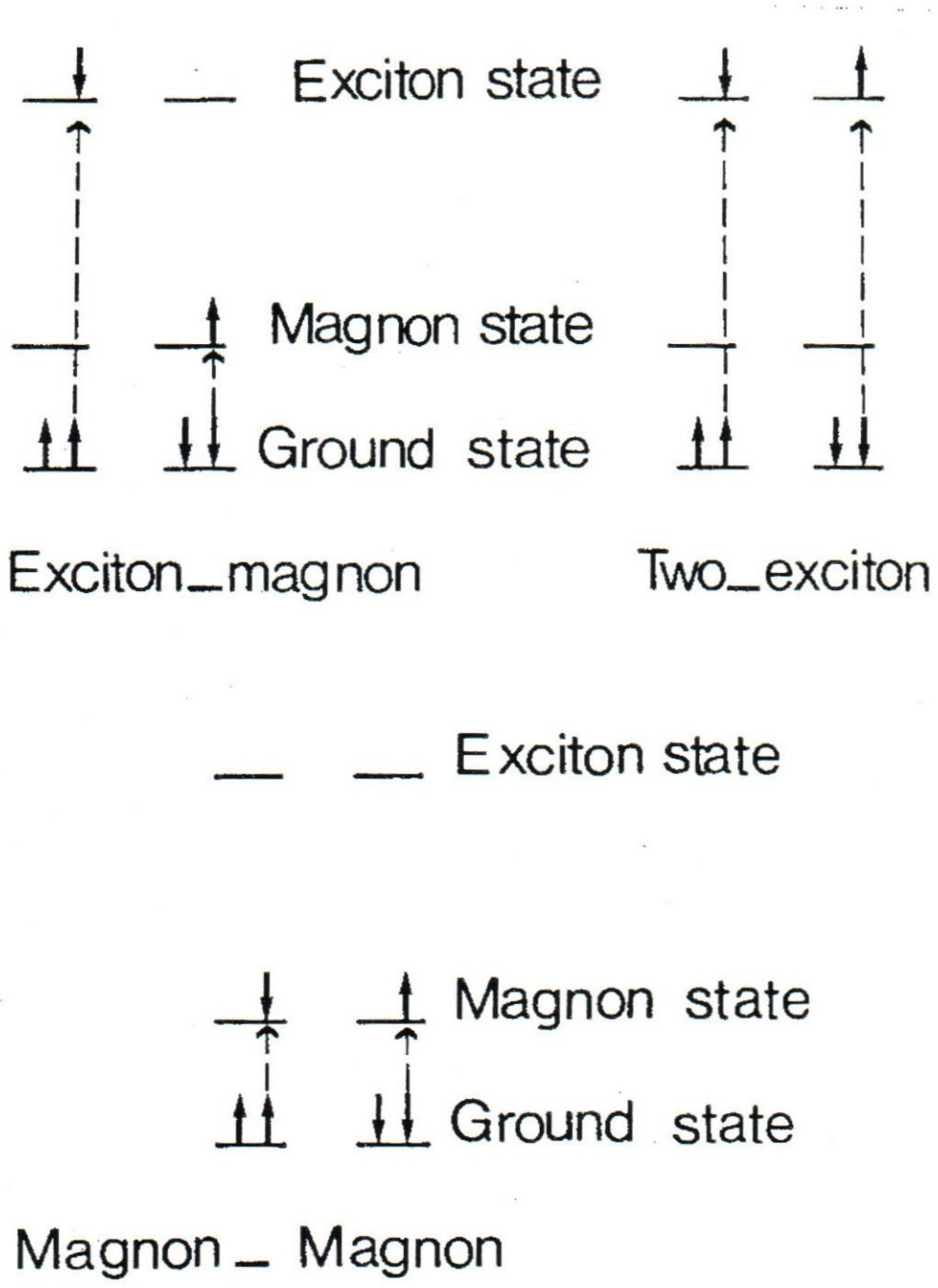

Figure (2.7): Schematic representation of exciton-magnon, exciton-exciton, magnon –magnon transitions [Ref. 6].

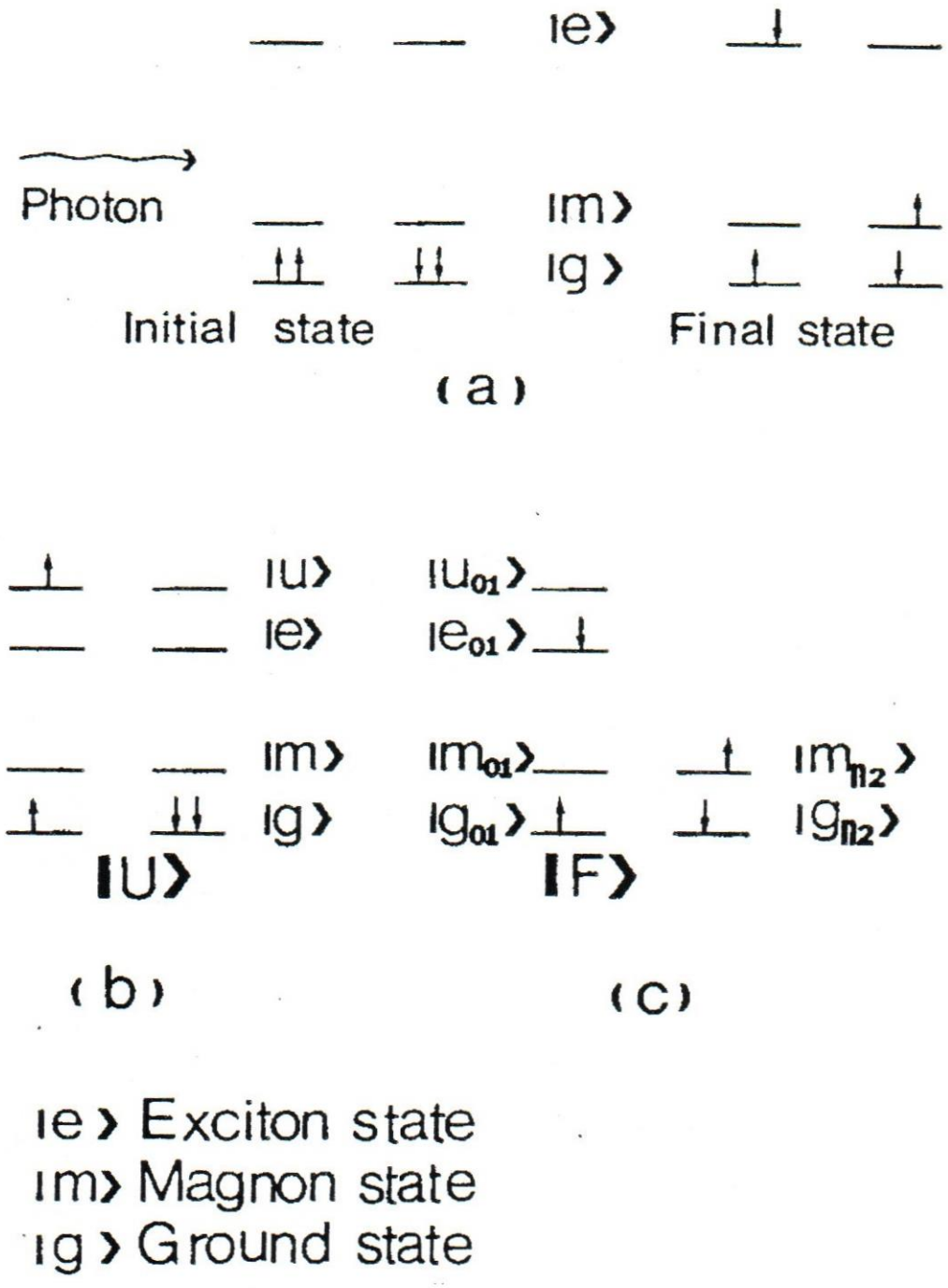

Figure (2.8): Schematic representation of exciton-magnon transition.

Now take the $\langle F|V|U\rangle$ term, which may be written as:

$$\langle F|V|U\rangle = \sum_{n=1}^{N} e^{iK\cdot\delta_{01,n2}} \langle e_{01} m_{n2}|V_{01,n2}|pu_{01} g_{n2}\rangle \qquad (2.8.5)$$

This term includes both sublattices as shown in figure (2.8.c). Where $\langle e_{01} m_{n2}|$ means that an exciton state on site 01 and a magnon state on site n2 (n refers to any other ion and number 2 represents down-sublattice), $|u_{01} g_{n2}\rangle$ means that the ground state on site n2 and an intermediate odd state on site 01, p is the permutation operator which leads to both direct and exchange term, $\delta_{01,n2}$ is the vector from site 01 to n2, and the sum is taken over all neighboring ions n.

If we take the direct term in the above equation:

$$\langle e_{01} m_{n2}|V_{01,n2}|u_{01} g_{n2}\rangle \qquad (2.8.6)$$

one can see that we have different M_s values on the same sublattice, i.e. g_{n2} has $M_s = -5/2$ and m_{n2} has $M_s = -3/2$. Therefore, this will violates the spin selection rule and becomes vanish.

But if an electronic exchange can take place between u_{01} and g_{n2}, i.e.

$$\langle e_{01} m_{n2}|V_{01,n2}|\overset{\frown}{u_{01} g_{n2}}\rangle \qquad (2.8.7)$$

This will avoid the violation of the spin selection rule. One can see this by considering just the spin parts as follows:

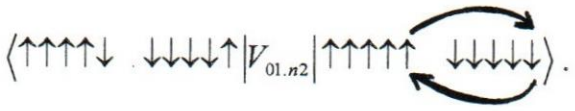

The bented arrows above indicates electron exchange between states on the opposite sublattices, and in this case we avoid violating the spin selection rule by having $\Delta S = 0$. From the above diagrams we see that the exchange term contributes for the exciton and magnon on the opposite sublattices [68]. It seems that the absorption bands are due to electric dipole transition carried through under the influence of an exchange interaction that couples both sublattices.

CHAPTER III

REVIEW OF EXPERIMENTAL RESULTS

In this chapter, the major experimental results in the literature are reviewed. The first section deals with the absorption spectra of $RbMnF_3$ and $KMnF_3$ were measured at various temperatures. Then in the following two sections, the band identifications of various bands and the observation of the line position shift are presented. In the last two sections, the D-band and the fine structure of the D-band are found at low temperatures and analyzed for the first time.

3.1 Spectrum of $KMnF_3$ and $RbMnF_3$

The optical absorption spectra of $RbMnF_3$ were studied [70] at 300 °K and 10 °K in the wavelength range of 2000 Å to 6000 Å, are shown in figures (3.1) and (3.2). The spectra of $KMnF_3$ are similar to those reported for $RbMnF_3$, except for slight displacement of energies of the various bands and some details of the fine structure of some of those bands at temperatures below T_N.

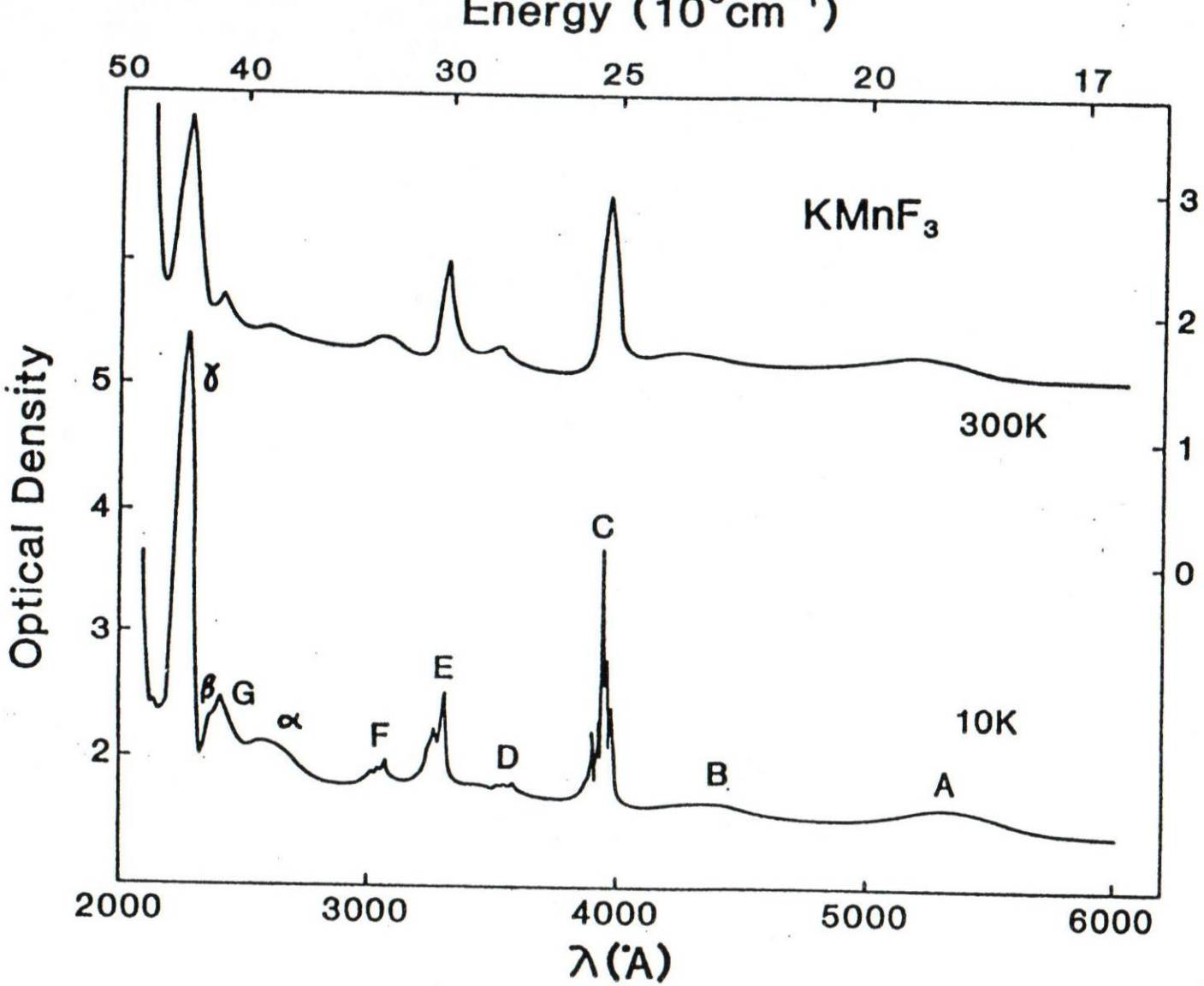

Figure (3.1): Absorption spectra of $KMnF_3$ at 300 °K and 10 °K. The Optical density $= \log_{10} I_0 / I = \alpha d / 2.303$, where d is the thickness of the sample [Ref. 71].

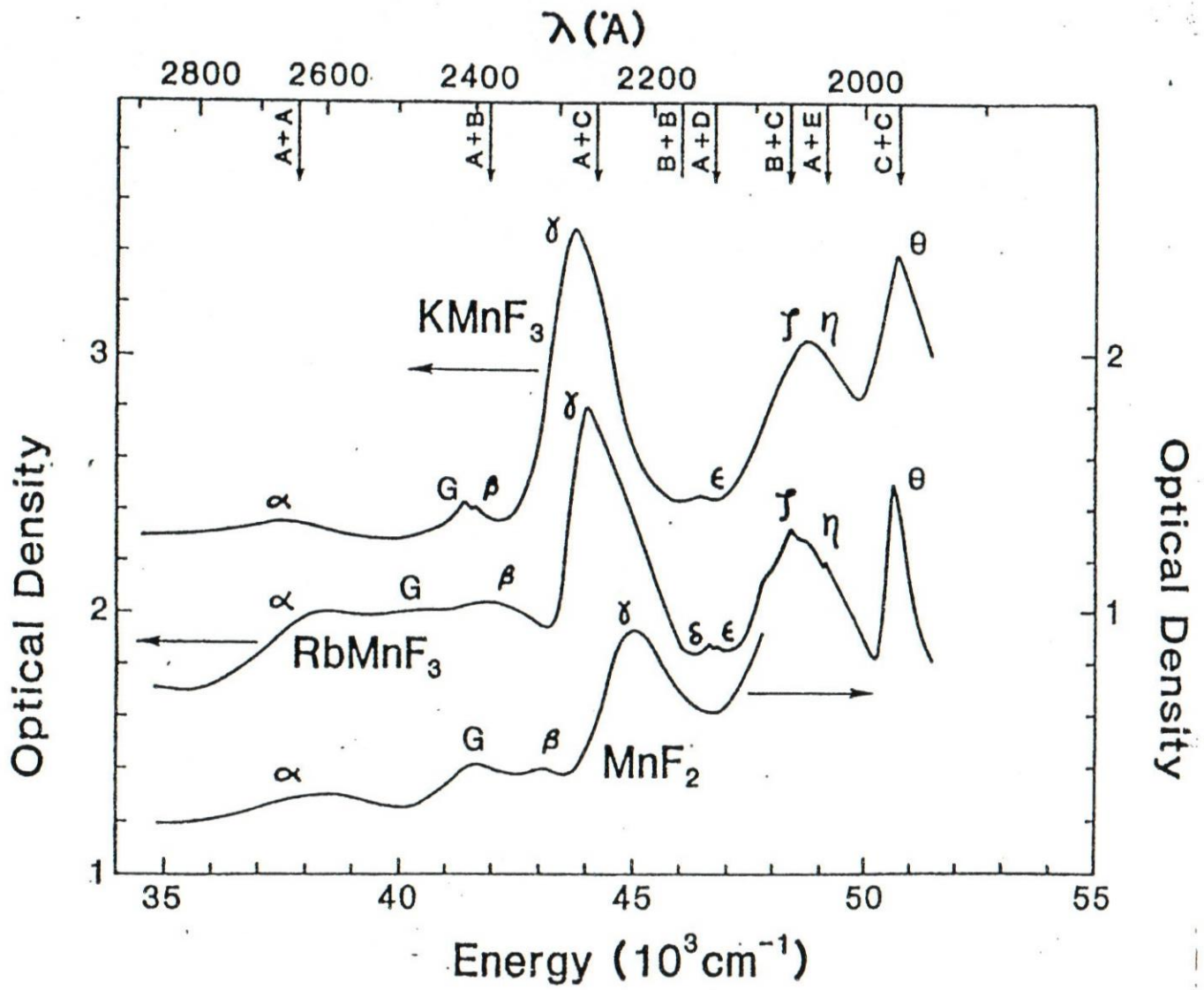

Figure (3.2): Absorption spectra of $KMnF_3$, $RbMnF_3$ at 10 °K in the UV region [Ref. 71].

3.2 Band Identification

The observed absorption bands as shown in figures (3.1) and (3.2) are classified into two major groups according to the temperature dependence of their intensities. The first group, are the magnon-exciton bands which are labelled as A, B, C, D... These bands are due to excitation from the ground state ${}^6A_{1g}$ of manganese ion (Mn^{2+}) to its quartet excited states like ${}^4T_{1g}(I), {}^4T_{2g}(I), {}^4A_{1g}+{}^4E_g(I), \ldots$ The second group, are the two-exciton bands, labelled $\alpha, \beta, \gamma, \ldots$ in order of increasing energies, and they respectively A+A, A+B, A+C... transitions.

3.3 Observation of Line Position Shift

The temperature dependence of the line positions of the some of the exciton-magnon bands in $RbMnF_3$ and $KMnF_3$ relative to their room temperature positions are shown in figures (3.3) and (3.4). They showed a drop in energy as temperature is raised to T_N and relatively little shift is observed above T_N. Table (3.1) shows the observed line position of some of transition bands in $RbMnF_3$.

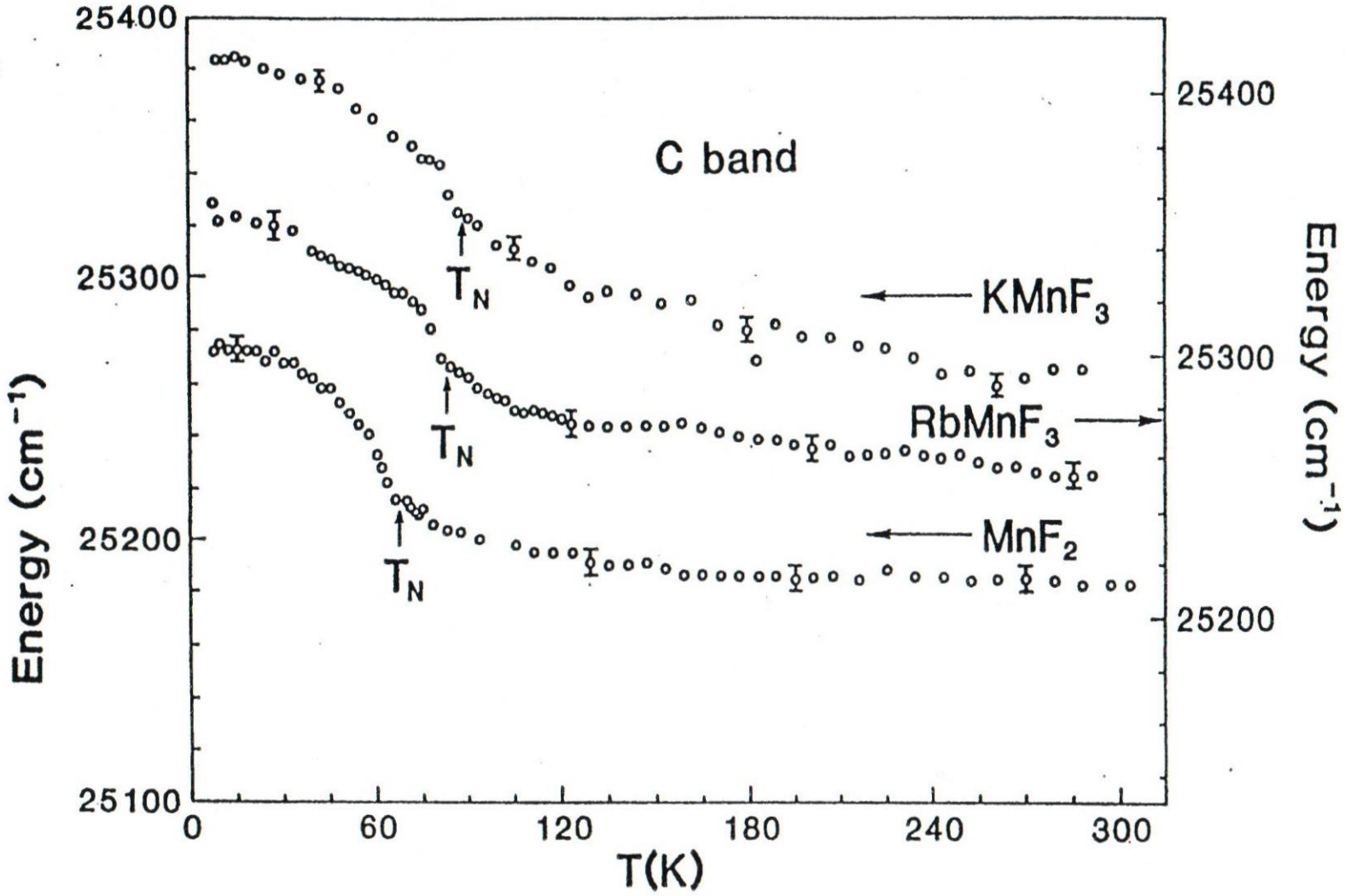

Figure (3.3): Temperature dependence of line positions of the C band in $KMnF_3$, $RbMnF_3$ [Ref. 71].

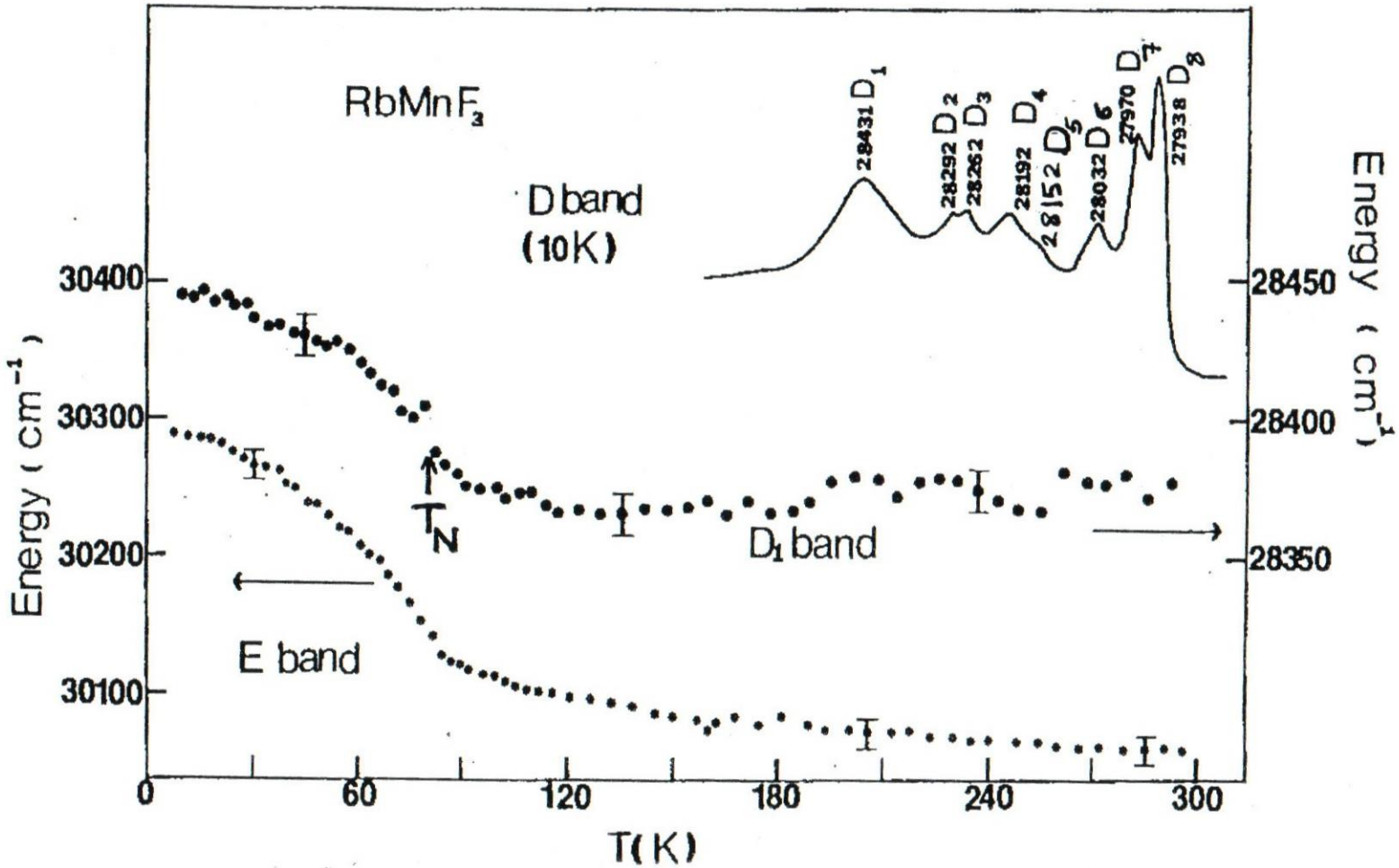

Figure (3.4): Temperature dependence of line positions of the D-Band and the absorption spectrum of band D in $RbMnF_3$ [Ref. 71].

This noticeable blue shift of energy levels below T_N, is explained by considering the exchange interaction between a pair of manganese ions (Mn^{2+}- Mn^{2+}) in magnetic crystals.

Table (3.1)

Observed Line Position of Some of Transition Bands in $RbMnF_3$.

Bands	Transitions	Observed Energy (cm^{-1})
A	${}^6A_{1g}({}^6s) \rightarrow {}^4T_{1g}({}^4G)$	19240
B	$\rightarrow {}^4T_{2g}({}^4G)$	23172
C	$\rightarrow {}^4A_{1g}({}^4G) + {}^4E_g({}^4G)$	25358
D	$\rightarrow {}^4T_{2g}({}^4D)$	28445
E	$\rightarrow {}^4E_g({}^4D)$	30290

3.4 The D-Band

The absorption spectrum of band D ($^4T_{2g}(^4D)$ state) in $RbMnF_3$ was observed in figure (3.4). This band is a exciton- magnon band [70] which is due to excitation from the ground state $^6A_{1g}$ of manganese ion (Mn^{2+}) to its quartet excited state $^4T_{2g}$ (Fig. 2.4).

The peak position as a function of temperature at ($10^\circ K$) was plotted. Figure (3.4) shows that the peak position shifts to a lower energy as the temperature is increased to T_N. The experimentally measured shift in figure (3.4) is about 70 cm^{-1}.

Since the line position of the D band showed no change as the temperature raised above T_N, figure (3.4) [71]. This band showed no phonon involved and therefore labeled as exciton-magnon band [65]. Its behavior above T_N is different from the behavior of the exciton-magnon-phonon bands like A and B bands, which are showed a shift to a higher energies when the temperature raised above T_N, figures (3.5) and (3.6) [71]. The peak positions of these bands showed an excellent fit with the expected behavior of the phonon-assisted transitions, which is given by the following equation:

$$E(T) = E(0) + \frac{A^*}{e^{T^*/T} - 1}$$

where E is the energy level with no vibrational effect, A^* is a constant and T^* is the characteristic temperature of a phonon with frequency ν_t ($kT^* = h\nu_t$, where k and h are, respectively, the Boltzman and planck's constants) [71].

The phonon modes involved in these bands have been determined by comparing the theoretical curves with the experimental curves as shown in Ref. 71.

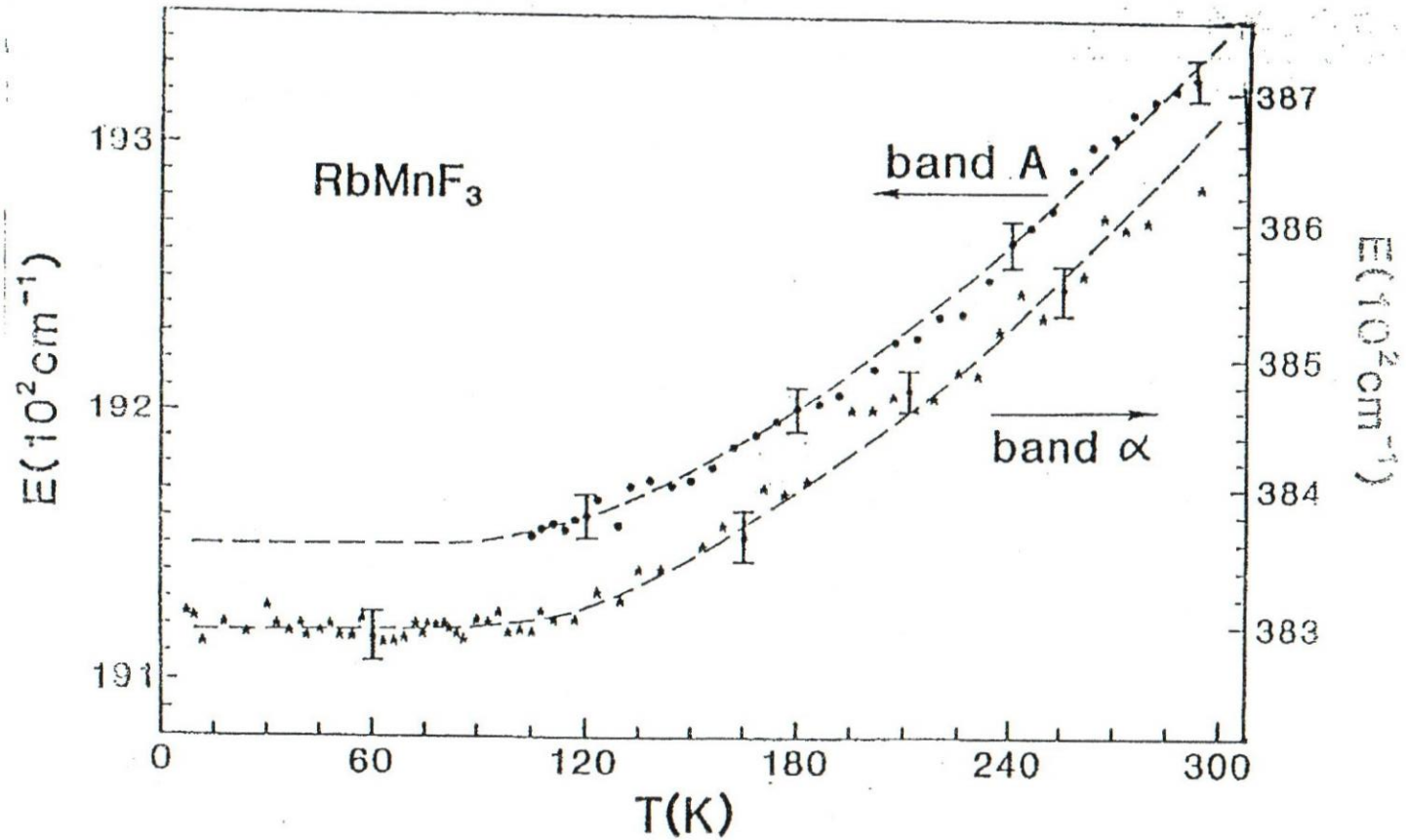

Figure (3.5): Temperature dependence of line positions of the A and α bands in $RbMnF_3$ [Ref. 71].

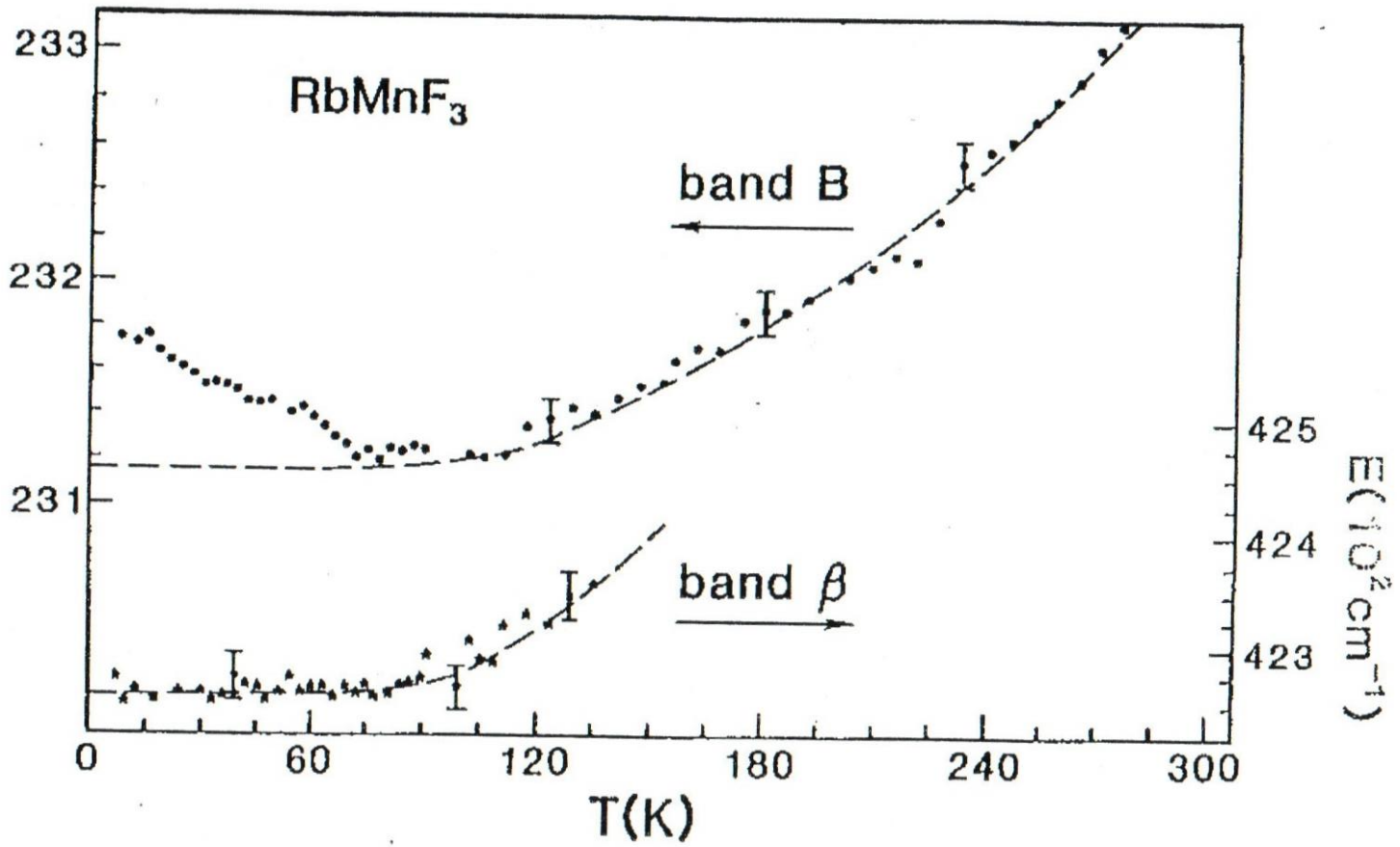

Figure (3.6): Temperature dependence of line positions of the B and β bands in $RbMnF_3$ [Ref. 71].

3.5 Fine Structure of the D-Band

Since my major interest is the D band (${}^6A_{1g} \rightarrow {}^4T_{2g}({}^4D)$), so I studied the spectrum of this band carefully.

The absorption spectrum of band D in $RbMnF_3$ was observed. As the temperature is lowered to $10^\circ K$, fine structure appears as shown in figure (3.4). The band is narrow and reveals at least eight individual lines. An interesting feature of the D band is that with the increase of the temperature, the separations between the peaks become smaller and each peak moves toward D_1. So the behavior of D_1-band describes the behavior of the total D-band. The line positions of the individual peaks are collected in Table (3.2).

The peak position shift observed in The D-band can be explained at least in part by considering the exchange interaction between a pair of manganese ions (Mn^{2+}) in magnetic crystals. At low temperature below T_N all spins are completely ordered and the exchange interaction is dominant as the temperature increases towards T_N, spin disorder takes place and the exchange interaction will be reduced. As the temperature increases above T_N a disappearance of these lines was noticeable (Fig. 3.4), which indicates that the exchange interaction between magnetic ions on opposite sublattices will vanishes at $T > T_N$ [72,26].

Table (3.2)

Observed Energy Levels of Band D (cm^{-1}) in The Low Temperature ($10^{\circ}K$) absorption Spectra of $RbMnF_3$.

Peak	Observed Energy (cm^{-1})
D_1	28431
D_2	28292
D_3	28262
D_4	28192
D_5	28152*
D_6	28032
D_7	27970
D_8	27938

[*: Means that this value was roughly estimated from figure (3.4)].

CHAPTER IV

THEORETICAL DISCUSSION

4.1 Spin - Orbital Coupling (L-S)

The effect of the spin-orbital coupling on the manganese ion Mn^{2+} results from the interaction between the spin and the angular momenta of the electrons [73].

The spin-orbital for d^n configurations in octahedral fields is shown as follows [74]:

$$H = \sum_i \left\{ \frac{-\hbar^2}{2m} \nabla_i^2 - \frac{Ze^2}{|r_i|} + \xi(r_i) \ell_i . s_i \right\} + \sum_{i>j} \frac{e^2}{|r_i - r_j|} + V_C \qquad (4.1.1)$$

So, the spin-orbital Hamiltonian form the above equation is:

$$H_{so} = \sum_i \xi(r_i) \ell_i . s_i \qquad (4.1.2)$$

where $\xi(r_i)$ is the single-electron spin orbit coupling parameter, which measures the strength of the interaction between the spin and orbital angular momentum of a single electron of the configuration [75].

The spin-orbital coupling will split each term into states, and successive states are specified by values of the total angular momentum (J) differing by unity. The number of states which arise from each term is (2 S + 1) for $S \leq l$ or $S > l$.

The energy for each state in the term due to spin-orbit interaction is given as [76]:

$$\overline{\Delta E} = \frac{\lambda}{2}[J(J+1) - L(L+1) - S(S+1)] \qquad (4.1.3)$$

where (J) is the total angular momentum, which is defined by $(\vec{J} = \vec{L} + \vec{S})$, and (λ) is the spin-orbit coupling constant and it's related to the single-electron spin-orbit coupling parameter (ξ) as following:

$$\lambda = \pm \frac{\xi_{nl}}{2S} \qquad (4.1.4)$$

The (+) sign holds for a shell less than half-full. And the (-) sign holds for a more-than half-full shell [77].

Therefore, we can calculate from (4.1.3) the separation in energy between the adjacent levels of a multiplet. If the quantum number

associated with the levels of lower energy is (J), the quantum number associated with the level of higher energy is (J+1), and the separation ΔE in the energy of the two levels is:

$$\Delta E_{J,J+1} = \overline{\Delta E}(L,S,J+1,M) - \overline{\Delta E}(L,S,J,M)$$

$$= \frac{\lambda}{2}\{[(J+1)(J+2) - L(L+1) - S(S+1)] - [J(J+1) - L(L+1) - S(S+1)]\}$$

$$\Delta E_{J,J+1} = \lambda(J+1) \qquad (4.1.5)$$

Thus we see that the separation ΔE in the energy of adjacent levels of a multiplet is proportional to the total angular momentum quantum number of the level of higher energy, this prediction is called the Land'e interval rule. The total width ΔE of a given multiplet can be evaluated [78]:

$$\Delta E = \lambda\ S\,(2L+1) \qquad (4.1.6)$$

The term notations for a particular states is given by the following symbol [79]:

$$^{(2s+1)}L_j,$$

where L denotes to the letter corresponding to the orbital angular momentum l value. And the number (2 s + 1) is called the multiplicity. For example, for $^3P_2$, we have $s=1$, $l=1$, and $j=2$.

If an atom contains two or more electrons that have common values of the quantum number n and l, because they are in the same sub shell, the exclusion principle which says simply that no two electrons can have the same set of all four quantum numbers, imposes restrictions on the possible values of the remaining quantum numbers. In LS coupling, the quantum numbers that are used, in addition to n and l for each electron, are l', s', j', m_j'. These quantum numbers specify the way the electrons interact in LS coupling.

So, to determine the LS coupling which satisfy the exclusion principle for manganese ion Mn^{2+}, which have five electrons in 3d sub shell. In table (4.1) we list part of the possible set of values of m_l and m_s for 5 electrons, which satisfy the exclusion principle. Let us suppose that our configuration includes a shell capable of holding N_0 electrons [equal to $2(2l+1)$, where l is the azimuthal quantum number], but containing in fact only N_1 electrons, where $N_1 < N_0$. Then the number of possible states is given as following [80]:

$$\frac{N_0!}{[N_1(N_0 - N_1)!]} \qquad (4.1.7)$$

So for $(3d^5)$ configuration, we have $N_0 = 10$ electrons and $N_1 = 5$ electrons, then according to Eq. (4.1.7) the number of possible states = $10!/[5!(10-5)!]$= 252 different sets of m_l and m_s. For each set the corresponding values of the quantum numbers m_l', m_s', m_j' are evaluated from the relations $m_l' = m_{l_1} + m_{l_2}, m_s' = m_{s_1} + m_{s_2}, m_j' = m_l' + m_s'$.

To identify the allowed quantum states, specified in table (4.1) in terms of m_l', m_s', m_j', with the specification of these states in terms of l', s', j', so for manganese ion Mn^{2+}, we have $(3d^5)$ configuration with n = 3, $l = 2$, and 5 electrons, each electron has $s = \frac{1}{2}$ i.e. $l_1 = l_2 = l_3 = l_4 = l_5 = 2$ and $s_1 = s_2 = s_3 = s_4 = s_5 = \frac{1}{2}$. Since $\vec{J} = \vec{L} + \vec{S}$, so the possible values of s', l' and j' given as following [81]:

$$s' = |s_1 - s_2|, |s_1 - s_2| + 1, \ldots\ldots\ldots, s_1 + s_2.$$

$$l' = |l_1 - l_2|, |l_1 - l_2| + 1, \ldots\ldots\ldots, l_1 + l_2. \qquad (4.1.8)$$

$$j' = |s - l|, |s - l| + 1, \ldots\ldots\ldots, s + l.$$

Therefore, a cording to Eq. (4.1.8), we conclude that the minimum value of s' is 1/2 and that the maximum value of s' is 5/2. So, the possible values are $s' = 1/2, 3/2, 5/2$. Also the minimum value of l' is 2, and the

maximum value of l' is 10. Therefore, the possible values are $l' = 2,3,4,5,6,7,8,9,10$, and the possible values of j' are then $j' = 3/2, 5/2, 7/2, 9/2, 11/2, 13/2, 15/2, 17/2, 19/2, 21/2, 23/2, 25/2$.

We find that the possible combinations of l', s', j', expressed in spectroscopic notation are as follows: $^2D, ^2F, ^2G, ^2H, ^2I, ^2K, ^2L, ^2M, ^2N, ^4D, ^4F, ^4G$ $^6H, ^6I, ^6K, ^6L, ^6M, ^6N, ^4H, ^4I, ^4K, ^4L, ^4M, ^4N, ^6D, ^6F, ^6G,$. And after applying exclusion principle the only possible quantum states for ($3d^5$) are those associated with the symbols [82]: $^2D, ^2P, ^2D, ^2F, ^2G, ^2H, ^2S, ^2D, ^2F, ^2G, ^2I, ^4P, ^4F, ^4D$ $, ^4G, ^6S$.

The effect of the spin-orbit coupling on the energy levels of Mn^{2+} is shown in figure (4.1). This figure is according to the above evaluations.

Table (4.1): Some possible quantum numbers for an ($3d^5$) configuration.

Entry	m_{l_1}	m_{l_2}	m_{l_3}	m_{l_4}	m_{l_5}	m_{s_1}	m_{s_2}	m_{s_3}	m_{s_4}	m_{s_5}	m_l'	m_s'	m_j'
1	+2	+2	+2	+2	+2	+1/2	+1/2	+1/2	+1/2	+1/2	+10	+5/2	+25/2
2	+2	+2	+2	+2	+2	+1/2	+1/2	+1/2	+1/2	-1/2	+10	+3/2	+23/2
3	+2	+2	+2	+2	+2	+1/2	+1/2	+1/2	-1/2	-1/2	+10	+1/2	+21/2
4	+2	+2	+2	+2	+2	+1/2	+1/2	-1/2	-1/2	-1/2	+10	-1/2	+19/2
5	+2	+2	+2	+2	+2	+1/2	-1/2	-1/2	-1/2	-1/2	+10	-3/2	+17/2
6	+2	+2	+2	+2	+1	-1/2	-1/2	-1/2	-1/2	-1/2	+9	-5/2	+13/2
7	+2	+2	+2	+1	+2	-1/2	-1/2	-1/2	-1/2	+1/2	+9	-3/2	+15/2
8	+2	+2	+2	+2	0	-1/2	-1/2	-1/2	+1/2	+1/2	+8	-1/2	+15/2
9	+2	+2	+2	+2	-1	-1/2	-1/2	+1/2	+1/2	+1/2	+7	+1/2	+15/2
10	+2	+2	+2	+2	-2	-1/2	+1/2	+1/2	-1/2	-1/2	+6	-1/2	+11/2
11	+2	+2	+2	0	+2	-1/2	-1/2	+1/2	+1/2	+1/2	+8	+1/2	+17/2
12	+2	+2	+2	-1	+2	-1/2	-1/2	-1/2	-1/2	-1/2	+7	-5/2	+9/2
13	+2	+2	+2	-2	+2	+1/2	+1/2	+1/2	+1/2	+1/2	+6	+5/2	+17/2
14	+2	+2	+2	+1	+1	-1/2	-1/2	-1/2	-1/2	+1/2	+8	-3/2	+13/2
15	+2	+2	+2	0	0	+1/2	+1/2	-1/2	-1/2	+1/2	+6	+1/2	+13/2
16	+2	+2	+2	-2	-2	-1/2	+1/2	-1/2	+1/2	-1/2	+2	-1/2	+3/2
17	-2	-2	-2	-2	-2	+1/2	-1/2	+1/2	-1/2	+1/2	-10	+1/2	-19/2
18	-2	-2	-2	-2	+2	-1/2	-1/2	-1/2	-1/2	+1/2	-8	-3/2	-19/2
.	.	.	.	.	.	.	.	.	.	.	.	.	.	.
.	.	.	.	.	.	.	.	.	.	.	.	.	.	.

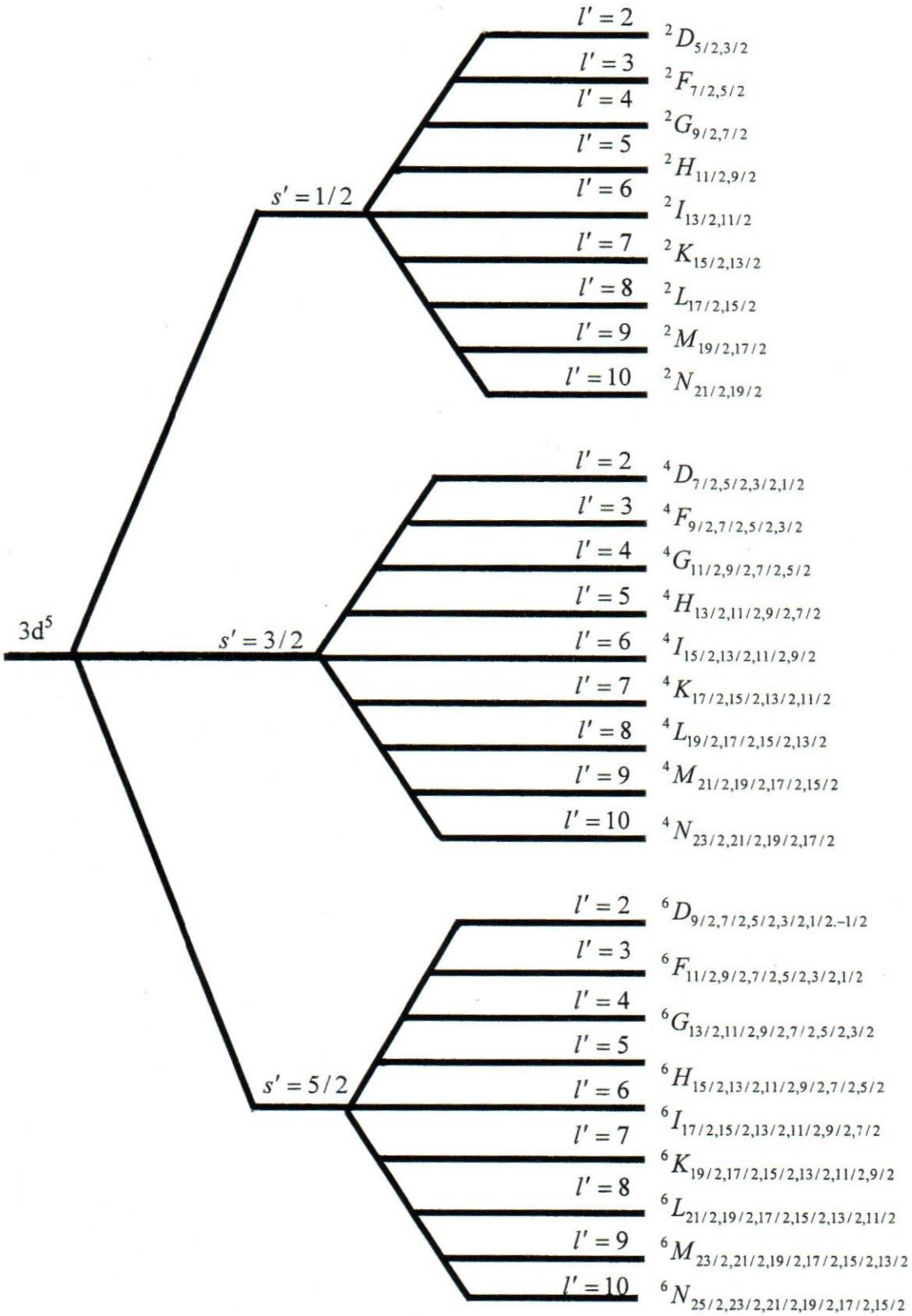

Figure (4.1): The splitting of the energy levels in a typical LS coupling configuration.

4.2 Energy Levels of D-Band

As shown from figure (4.1) ^4D-term splits into four levels due to spin-orbit interaction with $J = 1/2,3/2,5/2,7/2$. For ^4D-term we have $l = 2$, $s = 3/2$, So by using Eq. (4.1.4) we have $\lambda(^4D) = \frac{\xi_{3d}}{3}$. This yields using Eq. (4.1.3):

$$\overline{\Delta E_J} = -\frac{\xi_{3d}}{6}[J(j+1) - L(L+1) - S(S+1)] \qquad (4.2.1)$$

For ^4D:

$J = \frac{1}{2}$	$L = 2$	$S = \frac{3}{2}$	$\overline{\Delta E_{1/2}} = \frac{3}{2}\xi_{3d}$
$J = \frac{3}{2}$	$L = 2$	$S = \frac{3}{2}$	$\overline{\Delta E_{3/2}} = \xi_{3d}$
$J = \frac{5}{2}$	$L = 2$	$S = \frac{3}{2}$	$\overline{\Delta E_{5/2}} = \frac{\xi_{3d}}{6}$
$J = \frac{7}{2}$	$L = 2$	$S = \frac{3}{2}$	$\overline{\Delta E_{7/2}} = -\xi_{3d}$

The separation ΔE in energy between adjacent levels can be calculated by using Lande's interval rule (Eq. 4.1.5):

$$\Delta E_{J,J+1} = \lambda(J+1) = \frac{\xi_{3d}}{3}(J+1) \qquad (4.2.2)$$

This yield that:

$$J=\frac{1}{2} \qquad J+1=\frac{3}{2} \qquad \Delta E_{1/2,3/2}=\frac{\xi_{3d}}{2}$$

$$J=\frac{3}{2} \qquad J+1=\frac{5}{2} \qquad \Delta E_{3/2,5/2}=\frac{5\xi_{3d}}{6}$$

$$J=\frac{5}{2} \qquad J+1=\frac{7}{2} \qquad \Delta E_{5/2,7/2}=\frac{7\xi_{3d}}{6}$$

But for manganese ion (Mn^{2+}) $\xi_{3d}=300cm^{-1}$ [83], so the numerical values of the energies and separations and the total width of the ${}^4D$-term are given in Table (4.2). The energies and the separations between successive levels of ${}^4D$-term are shown in figure (4.2).

Table (4.2)

The calculated values of energies, separations, and the Total width of ^4D – term.

J	$\overline{\Delta E_J}(cm^{-1})$	$\Delta E_{J,J+1}(cm^{-1})$	The Total width of the ^4D -term (cm^{-1}).
$\frac{1}{2}$	450	150	
$\frac{3}{2}$	300	250	750
$\frac{5}{2}$	50	350	
$\frac{7}{2}$	-300		

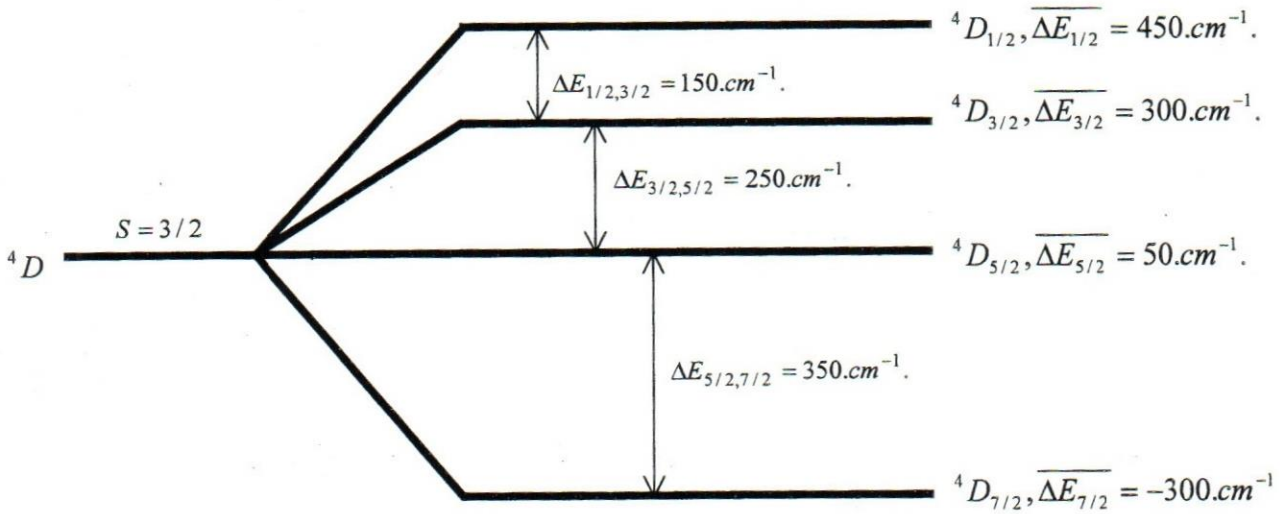

Figure (4.2): The splitting of the ^4D – term by spin-orbit coupling.

4.3 Exchange Interaction and Selection Rules

A careful study for the spectra of different Mn^{2+} compounds [6] showed that to explain the difference in intensities of the absorption bands between one manganese compound and another, one need to take into account the exchange interaction between the adjacent Mn^{2+} ions.

The spin-orbital coupling can produce a mixing between states of different spin multiplicity (for example, ${}^6A_{1g}({}^6s)$ and ${}^4T_{2g}({}^4D)$). In this case the selection rule can be broken down (i.e. $\Delta S = 0$) and the spin selection rule for a transition on one ion is relieved by exchange coupling with the neighboring ions [71,26].

Since there is no change in the line position with higher temperature the D-band in $RbMnF_3$ compound is an exciton-magnon band, i.e. excitations involving the simultaneous creation (or destruction) of an exciton and a magnon. Also the spin-orbit interaction splits ${}^4D$-band into four levels with different values of J (figure 4.2).

The interaction between the magnetic ions can be described in terms of the interactions between pairs of ions (i.e. exciton-magnon interaction). To illustrate how these interactions can take place, let us represent the pair interaction by a simple diagram as shown in figure (4.3).

A fine structure has been observed for the transitions to the ${}^4T_{2g}({}^4D)$ state (Fig. 3.4). The observed fine structure is attributed to an exchange interaction between ion pairs, taking into account the spin-orbit interaction of the ${}^4T_{2g}({}^4D)$ state.

Figure (3.4) shows that at low temperature the D-band reveals at least eight individual lines. To explain the appearance of these lines, I follow the same approach of the paper of Tanaka [84].

As discussed in chapter II, initially both ions are in the ground state $({}^6A({}^6S))$. Since we are dealing with an antiferromagnetic compound $RbMnF_3$ (i.e. spin up and spin down sublattices), the spin in the ground state for one ion is $5/2$ (spin up sublattice) and $-5/2$ (spin down sublattice) for another ion. And as the result of absorbing a photon they end up with an exciton state for one ion and a magnon state for the other ion.

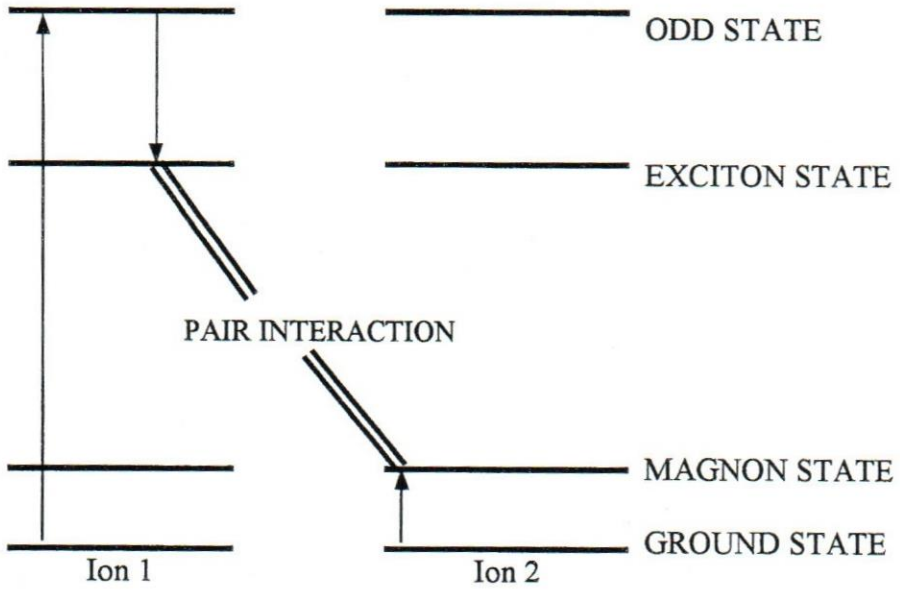

Figure (4.3): Schematic representation of the pair transition that causes magnon sidebands.

In the case where there is no internal field, all spin states are degenerate and two electronic orbital states are separated by an energy gap E_o. In the antiferromagnetic phase the exchange interaction develops and the exchange field lifts the degeneracy of spin states [84]. There can occur seven transition processes of interest as shown in figure (4.4). The splitting in the figure (4.4) are denoted by Δ_e and Δ_s, the first one is for the site

where the electronic orbital excitation takes place and the second for the site where only spin flip occurs. The Δ_{e_2} and Δ_{e_1} are molecular field splitting for the site where the electronic orbital excitation takes place [84].

Now let us consider the transitions between the terms of different spin-multiplicities, which are called intersystem combinations. Since the electric-dipole does not have matrix element between the states of different spin- multiplicity the intersystem combinations are forbidden. This selection rule is called spin-selection rule [85]. The selection rules between the intersystem combinations are:

$$\Delta s = 0,\pm 1$$
$$\Delta l = 0,\pm 1$$
$$\Delta j = 0,\pm 1 (j = 0 \not\rightarrow j = 0).$$

If we apply these selection rules on ion I (Fig. 4.4) we have 3 transition processes, where process 1 satisfy the $\Delta s = -1$, process 2 satisfy the $\Delta s = +1$ and process 3 satisfy the $\Delta s = 0$.

The spin selection rule can be overcome by exchange interaction between the two Mn^{2+} ions on the opposite sublattices as shown in figure (4.4). In this case the total spin of the two ions must be conserved. This condition is satisfied in the case of any of the four pairs of transition processes, (1,4), (1,7), (2,5) and (2,6); and of the process 3.

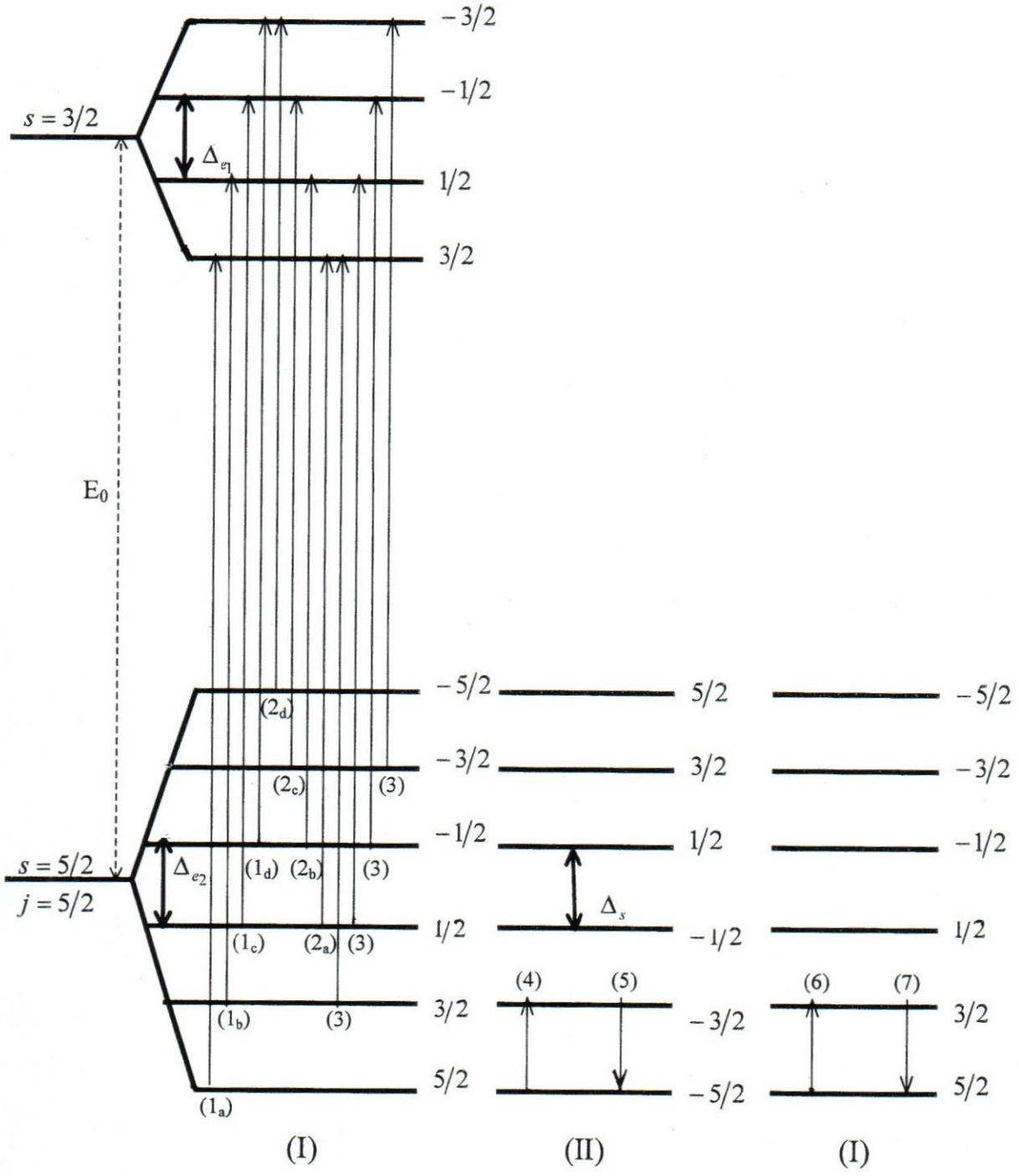

Figure (4.4): Transition processes in the molecular field description for $s = 5/2$ in the ground state and $s = 3/2$ in the excited state with I and II denoting the up and down sublattices, respectively.

The appearance of eight lines in the fine structure of D-band can be explained as follows:

The first pair and the second pair of transition processes can take place with the following frequencies:

$(1_a, 4), (1_a, 7)$ $$w = \left[E_0 + \frac{5}{2}\Delta_{e_2} - \frac{3}{2}\Delta_{e_1} \right] + \Delta_s$$

$(1_b, 4), (1_b, 7)$ $$w = \left[E_0 + \frac{3}{2}\Delta_{e_2} - \frac{1}{2}\Delta_{e_1} \right] + \Delta_s$$

$(1_c, 4), (1_c, 7)$ $$w = \left[E_0 + \frac{1}{2}\Delta_{e_2} + \frac{1}{2}\Delta_{e_1} \right] + \Delta_s$$

$(1_d, 4), (1_d, 7)$ $$w = \left[E_0 - \frac{1}{2}\Delta_{e_2} + \frac{3}{2}\Delta_{e_1} \right] + \Delta_s$$

The other pairs of transition processes can take place with the following frequencies:

$(2_a, 5), (2_a, 6)$ $$w = \left[E_0 + \frac{1}{2}\Delta_{e_2} - \frac{3}{2}\Delta_{e_1} \right] - \Delta_s$$

$(2_b, 5), (2_b, 6)$ $$w = \left[E_0 - \frac{1}{2}\Delta_{e_2} - \frac{1}{2}\Delta_{e_1} \right] - \Delta_s$$

$(2_c, 5), (2_c, 6)$ $$w = \left[E_0 - \frac{3}{2}\Delta_{e_2} + \frac{1}{2}\Delta_{e_1} \right] - \Delta_s$$

$(2_d, 5), (2_d, 6)$ $$w = \left[E_0 - \frac{5}{2}\Delta_{e_2} + \frac{3}{2}\Delta_{e_1} \right] - \Delta_s$$

As we see from the above we have eight peaks (transitions) with eight frequencies and this explain the appearance of eight lines in the fine structure of D-band. The process 3 gives the total band at $w = E_0$ which appears as the temperature approaches T_N, because the sublattice magnetization gets smaller, so the separations between eight peaks become smaller and each frequency tends to E_0.

4.4 Transition Mechanisms

Mechanism that causes the appearance of the fine structure in ${}^4T_{2g}({}^4D)$ transition in $RbMnF_3$ is not well understood.

In the first place, let us consider the vibronic interaction, the vibronic mechanism was discussed previously which relaxes the parity selection rule. The experimental results in figure (3.4) shows that the behavior of the D-band above T_N is different from the expected behavior of phonon-assisted transitions, where a shift in line position is expected above T_N [71], this implies the involvement of other mechanism in the transition.

A second possibility is due to spin-orbit interaction. Spin-orbit interaction can overcome the spin selection rules, because it mixes states of different spin multiplicity. But the energy spacing calculated by means of

spin-orbit interaction does not fit the spacing between the peak lines obtained in experimental data. So we may conclude that spin-orbit interaction is not the only mechanism involved in the appearance of the fine structure of the D-band in $RbMnF_3$.

A third possibility is a cooperative mechanism involving exchange interaction between adjacent Mn^{2+} ions. For this mechanism our analysis in the previous section show that the transitions to the ${}^4T_{2g}({}^4D)$ state are almost caused by the exchange interaction i.e. the spin and parity selection rules are lifted by the exchange interaction between a pair of Mn^{2+} ions. Because it fits the appearance of eight lines in the fine structure of the D-band in $RbMnF_3$. Also, below T_N the D-band showed a total shift ($70cm^{-1}$) as a function of the temperature. Exchange field in the magnetically ordered state causes this shift. The exchange field is proportional to the sublattice magnetization, decreases with increases temperature and vanishes at T_N i.e. the peaks disappearance was observed in the spectrum of the D-band (Fig. 3.4) at $T > T_N$, which indicates spin disorder. And this supports the idea that the exchange mechanism plays an essential role in breaking the spin selection rule and making the forbidden transitions to be allowed in this crystal.

CHAPTER V

SUMMARY OF MAJOR RESULTS

The optical spectrum of $RbMnF_3$ compound has been studied, and most of the major absorption bands have been identified and attributed to $d^5 \rightarrow d^5$ transitions of Mn^{2+}. These transitions are due to partially allowed electric dipole transitions that are strongly forbidden by spin and parity selection rules. The breaking of the parity and spin selection rules leads to four possible mechanisms for electric dipole transitions. These mechanisms are:

1- Vibronic / Spin-orbit.

2- Vibronic / Exchange.

3- Exchange / Spin-orbit.

4- Fully exchange mechanism.

The fine structure of the exciton-magnon D-band of Mn^{2+} magnets in the absorption spectra of $RbMnF_3$ are studied and analyzed by examining the above mechanisms. And the following major results are obtained:

1- In $RbMnF_3$, fine structure in the D-band was observed at low temperature.

2- The position line of the D-band shows no change when the temperature raised above T_N, which indicates that there is no phonon involvement. So this band is labeled as exciton-magnon band.

3- The spin-orbit calculations do not give the expected energy difference between the peaks, and did not give the right number of observed peaks. We may conclude that the spin-orbit interaction is not the only mechanism involved in the appearance of the fine structure of the D-band in $RbMnF_3$.

4- The dominant mechanism for the transitions to states arising from the free ion ^4D term with symmetry $^4T_{2g}(^4D)$ in $RbMnF_3$ is the exchange mechanism (mechanism 4). This means that the spin and parity selection rules are both broken by the exchange interaction between Mn^{2+} ions.

5- The disappearance of the fine structure peaks at $T > T_N$ also proves that the exchange interaction is dominant at low temperature (i.e. $T < T_N$) and it reduces when the temperature is increased toward T_N.

REFERENCES

1. D.R. Huffman , R.L. Wild and M. Shinmei, J. Phys. 50, (1969) 4092.
2. M.Yokogawa, K. Taniguchi and C. Hamaguchi: Solid State Commun.19, 261 (1976).
3. J.W. Stout. J. Chem. Phys. 31, 709 (1959).
4. D.H. Goode, J. Chem. Phys. 43, 2830 (1965).
5. J. Ferguson, W.J. Guggenheim and Y. Tanabe, J. Phys. Soc. Japan 21, 692 (1966).
6. L.L. Lohr, Jr. and D.S. McClure, J. Chem. Phys. 49, 3516 (1968).
7. S. Koide and M.H.L. Pryce, Phil. Mag. 3, 607 (1958).
8. J. Ferguson, H.J. Guggenheim and Y. Tanabe, J. Appl. Phys. 36, 1046 (1965).
9. D.D. Sell, R.L. Green and R.M. White, Phys. Rev. 158, 489 (1967).
10. Y. Tanabe and K.I. Gondaira, J. Phys. Soc. Japan 22, 489 (1967).
11. D.E. McCumber and M.D. Sturge, J. Applied Phys. 34, 1682 (1963).
12. G.F. Imbusch, W.m. Yen, A.L. Schawlow, D.E. McCumber and M.D Sturge, Phys. Rev. 133, A1029 (1964).

13. J. Woods Halley and I. Silvera, Phys. Rev. Letters 15, 654 (1965); Phys. Rev. 149, 415 (1966); 149, 423 (1966).

14. S.J. Allen, Jr., R. Loudon and P.L. Richards, Phys. Rev. Letters 16, 463 (1966).

15. R.L. Green , D.D. Sell, W.M. Yen, A.L. Schawlow and R.M. White, Phys. Rev. Letters 15, 656 (1965).

16. R.S. Meltzer, M. Lowe and D.S. McClure, Phys. Rev. 180, 561 (1969).

17. J. Ferguson, Australian J. Chem. 21, 307 (1968).

18. J.P. Vander Ziel and H.J. Guggenheim, Phys. Rev. 166, 479 (1968).

19. K. Motizuki and Harada, Solid State Commun. 8,951 (1970); Progr. Theor. Phys. Supp. No. 46,40 (1970).

20. I. Harada and K. Motizuki, J. Phys. Soc. Japan 32, 927 (1972).

21. D.R.Huffman, J. Appl. Phys. 40, 1334 (1969).

22. H. Tanaka, J. Phys. Soc. Japan 31, 368 (1971).

23. K. Shinsawa and Y. Tanabe, J. Phys. Soc. Japan 30, 1280 (1971).

24. T. Fujiwara and Y. Tanabe, J. Phys. Soc. Japan 32, 912 (1972).

25. M.S. Seehra and S. Abumansoor, Solid State Coommun. 56, 97 (1985).

26. H.J.W.M. Hoekstra, H.F. Folkersma and C. Haas: Solid State Commun. 51, 657 (1984).

27. D.D. Sell, J. Applied Phys. 39, 1030 (1968).

28. A.V. Malakhovskii, G.G. Vasilev, and T.P. Morozova Phys. Stat. Sol. (b) 138, 285 (1986).

29. C.G. Windsor and R.W.H. Stevenson, Proc. Phys. Soc. (London) 87, 501 (1966).

30. E.U. Condon and G.H. Shortly, The Theory of Atomic Spectra (Cambridge University Press, London, 1960) P.177.

31. S. Sugano, Y. Tanabe, and H. Kamimura, Multiplets of Transition-Metal Ions in Crystals (Academic Press, New York and London, 1970) P. 62-64.

32. C.J. Ballhausen, Introduction to Ligand Field Theory (McGraw-Hill, New York, 1962).

33. G. Racah, Phys. Rev. 62, 438 (1942).

34. B.N. Figgs, Introduction to Ligand Fields (Interscience Publisher, New York, London, Sydney, 1966) P. 8-12.

35. Bethe, Ann. Phys., 3 133 (1929).

36. Ref. 32.

37. J.S. Griffith, The Theory of Transion-Metal Ion (Cambridge University Press, London, 1960).

38. W. Low, Paramagnetic Resonance in Solids (Academic Press, New York, 1960).

39. L.E. Orgel, J. Chem. Phys. 23, 1004 (1952).

40. Y. Tanabe and S. Sugano, J. Phys. Soc. Japan 9, 753 (1954).

41. S. Koide and M.H.L. Pryce, Phil. Mag. 3, 607 (1958).

42. Ref. 32, p. 60.

43. Ref. 37, p. 204.

44. Ref. 34, p. 37.

45. Ref. 34, p. 33.

46. Ref. 32, p. 64.

47. L.E. Orgel, J. Chem. Phys. 23, 1004 (1952).

48. Tanabe and Sugano, J. Phys. Soc. Japan 9, 753 (1954).

49. W. Low and G. Rosengarten, J. Mol. Spectry. 12, 319 (1964).

50. John C. Slater,The Self-Consistent Field for Molecules and Solids, Quantum Theory of Molecules and Solids (McGraw-Hill, New York, London, Sydney, 1974).

51. Ref. 37, p. 46.

52. Stephen Gasiorowicz, Quantum Physics (John Wiley and Sons, New York, 1996) p. 346.

53. E.E. Anderson, Modern Physics and Quantum Mechanics (W.B. Saunders, Philadelphia, 1971) p. 351.

54. J.D. Jackson, Classical Electrodynamics (John Wiley and Sons, New York, 1962) p. 397.

55. Richard L. Liboff, Introductory Quantum Mechanics (1990).

56. Ref. 37, p. 54-55.

57. Ref. 36, p. 353.

58. Ref. 32, p. 32.

59. M. Weissbluth, Atoms and Molecules (Academic Press, New York, 1978) p. 502.

60. D. Bohm, Quantum Theory (Prentice-Hall, New York, 1951) p. 436.

61. J.H. Van Vleck, J. Phys. Chem. 41,64 (1937)

62. Ref. 32, p. 186.

63. Ref. 53, p. 186.

64. F.A. Cotton, Chemical Applications of Group Theory (Interscience Publishers, New York, 1963) p. 209.

65. G. Herzberg, Infrared and Ramman Spectra (D. Van Nostrand Co., Inc., New York, 1945) p. 122.

66. Y. Tanabe, T. Moriya, and Sugano, Phys. Rev. Letters, 15, 1023 (1965).

67. K. Gondaira and Y. Tanabe, J. Phys. Soc. Japan, 21, 1527 (1966).

68. D.D. Sell, R.L. Green and R.M. White, Phys. Rev. 158, 489 (1967).

69. S.J. Allen, Jr., R. Loudon and P.L. Richards, Phys. Rev. Letters 16, 463 (1966).

70. J. Ferguson, Australian J. Chem. 21, 307 (1968).

71. S. Darwish, Mohindar S. Seehra, Phys. Rev B, 37, 3422 (1988).

72. H.J.W.M. Hoekstra, P.R. Boudewijn, H. Groenier and C. Haas (1982).

73. R. Eisberg and R. Resnick, Quantum Physics of Atoms, Molecules, Solids, Nuclei and Particles, (1974).

74. Ref. 32, p. 120.

75. Ref. 34, p. 57.

76. Gerald Burns, Solid State Physics (Academic Press, New York, London, Sydney, 1985).

77. Ref. 34, p. 58.

78. Ref. 32, p. 28-29.

79. Ref. 55, p. 683.

80. John C. Slater, Quantum Theory of Atomic Structure, Volume I (McGraw-Hill, New York, 1960).

81. Ref. 73, p. 389.

82. Ref. 55, p. 588.

83. Ref. 34, p. 60.

84. H. Tanaka, J. Phys. Soc. Japan, 31, 368 (1971).

85. S. Sugano, Y. Tanabe, and H. Kamimura, Multiplets of Transition-Metal Ions in Crystals (Academic Press, New York and London, 1970) P. 115-116.

86. Thomas M. Dunn, Some Aspects of Crystal Field Theory (Harper and Row, New York, 1965) P. 10.

APPENDIX (A)

Slater Integrals (Slater-Condon Parameters):

$$F^K(dd) = \int_0^\infty r_1^2 dr_1 \int_0^\infty r_2^2 dr_2 R_d^2(r_1) R_d^2(r_2) \frac{r_<^K}{r_>^{K+1}} \qquad \text{(A.1)}$$

Where ($r_<$) is the lesser and ($r_>$) is the greater of (r_1) and (r_2).

The Slater- Condon parameters are equal to:

$$F_0 = F^0, F_2 = \frac{1}{49} F^2, and. F_4 = \frac{1}{441} F^2 \qquad \text{(A.2)}$$

APPENDIX (B)

Crystal Potential of Octahedral Field

The potential at a point P inside the octahedral as shown in Fig (B.1) can be evaluated as follows [86]. The potential at point p due to charge 1 is:

$$V_1 = \frac{ze^2}{d} \tag{B.1}$$

Where d is the distance between charge 1 and point p and may be written as:

$$d = \sqrt{a^2 + r^2 - 2ar\cos\theta} = a\sqrt{1 + \left(r/a\right)^2 - 2\left(r/a\right)\cos\theta}.$$

Expressing this in terms of Legendre polynomials assuming r < a, we have

$$\frac{1}{d} = \frac{1}{a\sqrt{1 + \left(r/a\right)^2 - 2\left(r/a\right)\cos\theta}} = \sum_{l=0}^{\infty} p_l(\cos\theta)\left(\frac{r}{a}\right)^l \tag{B.2}$$

$$V_1 = \frac{ze^2}{a}\sum_{l=0}^{\infty} p_l(\cos\theta)\left(\frac{r}{a}\right)^l . \tag{B.3}$$

The values for $p_l(\cos\theta)$ are:

$$\begin{aligned} p_0(\cos\theta) &= 1 \\ p_1(\cos\theta) &= \cos\theta \\ p_2(\cos\theta) &= 3\cos^2\theta - 1 \\ p_3(\cos\theta) &= \frac{1}{2}\left(5\cos^3\theta - 3\cos\theta\right) \\ p_4(\cos\theta) &= \frac{1}{8}\left(35\cos^4\theta - 30\cos^2 + 3\right) \end{aligned} \tag{B.4}$$

.terms with $l > 4$ are not necessary, since their contribution will be very small.

$$V_1 = \left[1 + \left(\frac{r}{a}\right)p_1(\cos\theta) + \left(\frac{r}{a}\right)^2 p_2(\cos\theta) + \left(\frac{r}{a}\right)^3 p_3(\cos\theta) + \left(\frac{r}{a}\right)^4 p_4(\cos\theta)\right] \tag{B.5}$$

using $\cos^n(\theta + \pi) = -\cos^n\theta$ for n odd we can write

$$V_1 + V_2 = \frac{ze^2}{a}\left[1 + \left(\frac{r}{a}\right)^2 p_2(\cos\theta) + \left(\frac{r}{a}\right)^4 p_4(\cos\theta)\right] \tag{B.6}$$

where V_2 is the potential at point p due to charge 2.

Substituting for $p_l(\cos\theta)$ and putting $\cos\theta = z/r$

$$V_1 + V_2 = \frac{Ze^2}{a}\left[1 + \frac{1}{2}\left(\frac{r}{a}\right)\left(\frac{3z^2}{r^2} - 1\right) + \frac{1}{8}\left(\frac{r}{a}\right)^4\left(\frac{35z^4}{r^4} - \frac{30z^2}{r^2} + 3\right)\right] \tag{B.7}$$

similarly,

$$V_3 + V_4 = \frac{Ze^2}{a}\left[1+\frac{1}{2}\left(\frac{r}{a}\right)\left(\frac{3x^2}{r^2}-1\right)+\frac{1}{8}\left(\frac{r}{a}\right)^4\left(\frac{35x^4}{r^4}-\frac{30x^2}{r^2}+3\right)\right] \tag{B.8}$$

and the same for $V_5 + V_6$ with x changed to y

$$V = \sum_{i=1}^{6} V_i = 6\frac{Ze^2}{a}+\frac{35Ze^2}{4a^5}\left(x^4+y^4+z^4-\frac{3}{5}r^4\right)$$

$$= 6\frac{Ze^2}{a}+D\left(x^4+y^4+z^4-\frac{3}{5}r^4\right) \tag{B.9}$$

where $D = \frac{35Ze^2}{4a^5}$.

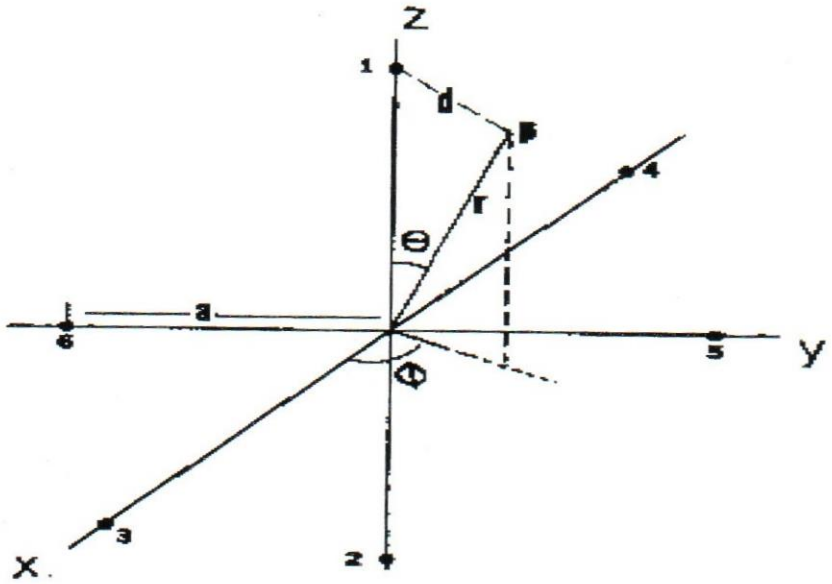

Figure (B.1): Evaluation of the crystal field potential at point p inside an octahedral of negative charges [Ref. 34].

APPENDIX (C)

Energy - Level Splitting for d^1 in Octahedral Field

The octahedral potential expressed in terms of spherical harmonics from Eq (2.5.2) is:

$$V_C = \frac{7Ze^2}{3a^5}\sqrt{\pi}\, r^4\left[Y_4^0 + \sqrt{5/14}\left(Y_4^4 + Y_4^{-4}\right)\right] \tag{C.1}$$

and the first order-energy is given by:

$$\int \psi^* V_C \psi d\tau \equiv < \psi | V | \psi > \tag{C.2}$$

where ψ is the atomic wave function for the the d state and may be written in terms of spherical harmonics as:

$$\psi = R_{n,l}(r) Y_l^m(\theta, \phi). \tag{C.3}$$

using (C.1) and (C.3), (C.2) may be written as:

$$\frac{7Ze^2}{3a^5}\sqrt{\pi} < R_{n,l'}(r) | r^4 | R_{n,l}(r) > \left[< Y_{l'}^{m'} | Y_4^0 | Y_l^m > + \sqrt{15/4}\left(< Y_{l'}^{m'} | Y_4^4 | Y_l^m > + < Y_{l'}^{m'} | Y_4^{-4} | Y_l^m > \right)\right].$$

...(C.4)

$l = 2$ for the d functions but m takes on values $\pm 2, \pm 1, 0$.

The evaluation can be done by the use of the Gaunt formula [80].

$$< Y_{l'}^{m'} \left| Y_L^M \right| Y_l^m >= (-1)^{m'} \sqrt{(2l'+1)(2L+1)(2l+1)/4\pi} \; X \begin{pmatrix} l' & L & l & l' & L & l \\ -m & M & m & 0 & 0 & 0 \end{pmatrix}$$

...(C.5)

which is non vanishing only when:

$$\begin{aligned} &-m' + M + m = 0 \\ &l' + L + l = even \;\; number. \end{aligned} \qquad \text{(C.6)}$$

The evaluation is simplified by the use of a defined quantity $C^K(lm, l'm')$a

$$C^K(lm, l'm') = \sqrt{4\pi/(2K+1)} < Y_{l'}^{m'} \left| Y_L^M \right| Y_l^m > . \qquad \text{(C.7)}$$

The values of $C^K(lm, l'm')$ are given in Table (C.1) [80] for the s, p, and d electrons.

The evaluation of Equation (C.4) can be done easily, with the use of (C.7) and Table (C.1)[80]. For example, when $m_l = m_l' = 2$ Equation (C.4) reduces to:

$$\frac{7Ze^2\sqrt{\pi}}{3a^5} < R_{2,2}(r)|r^4|R_{2,2}(r) >< Y_2^2|Y_4^0|Y_2^2 >$$

$$= \frac{7Ze^2\sqrt{\pi}}{3a^5} < R_{2,2}(r)|r^4|R_{2,2}(r) > \sqrt{9/4\pi}\sqrt{1/441}$$

$$= \frac{1}{6}\frac{Ze^2}{a^5} < R_{2,2}(r)|r^4|R_{2,2}(r) >$$

$$= Dq \qquad (C.8)$$

where D and q are defined by (2.5.5) as

$$D = \frac{35Ze^2}{4a^5} \text{ and } q = \frac{2}{105}\int_0^\infty R_{n,l}^*(r).r^4.R_{n,l}(r)r^2dr.$$

similar evaluations for the other non-vanishing matrix elements are done and the results are:

$$< \psi(-2)|V_C|\psi(2) >=< \psi(2)|V_C|\psi(-2) >= 5Dq,$$

$$< \psi(1)|V_C|\psi(1) >=< \psi(-1)|V_C|\psi(-1) >= -4Dq,$$

$$< \psi(0)|V_C|\psi(0) >= 6Dq,$$

where $\psi(M_L)$ is used to denote the particular component of the fivefold degenerate wave functions.

Table C.1

$C^K(lm,l'm')$ Values [Ref. 80].

	m	m'	K				
			0	1	2	3	4
ss	0	0	1	0	0	0	0
sp	0	±1	0	$-\sqrt{1/3}$	0	0	0
	0	0	0	$\sqrt{1/3}$	0	0	0
pp	±1	±1	1	0	$-\sqrt{1/25}$	0	0
	±1	0	0	0	$-\sqrt{3/25}$	0	0
	±1	∓1	0	0	$-\sqrt{6/25}$	0	0
	0	0	1	0	$\sqrt{4/25}$	0	0
sd	0	±2	0	0	$\sqrt{1/5}$	0	0
	0	±1	0	0	$-\sqrt{1/5}$	0	0
	0	0	0	0	$\sqrt{1/5}$	0	0
pd	±1	±2	0	$-\sqrt{6/15}$	0	$\sqrt{3/245}$	0
	±1	±1	0	$\sqrt{3/15}$	0	$-\sqrt{9/245}$	0
	±1	0	0	$-\sqrt{1/15}$	0	$\sqrt{18/245}$	0
	±1	∓1	0	0	0	$-\sqrt{30/245}$	0

	±1	∓2	0	0	0	$\sqrt{45/245}$	0
	0	±2	0	0	0	$\sqrt{15/245}$	0
	0	±1	0	$-\sqrt{3/15}$	0	$-\sqrt{24/245}$	0
	0	0	0	$\sqrt{4/15}$	0	$\sqrt{27/245}$	0
dd	±2	±2	1	0	$-\sqrt{4/49}$	0	$\sqrt{1/441}$
	±2	±1	0	0	$\sqrt{6/49}$	0	$-\sqrt{5/441}$
	±2	0	0	0	$-\sqrt{4/49}$	0	$\sqrt{15/441}$
	±2	∓1	0	0	0	0	$-\sqrt{35/441}$
	±2	∓2	0	0	0	0	$\sqrt{70/441}$
	±1	±1	1	0	$\sqrt{1/49}$	0	$-\sqrt{16/441}$
	±1	0	0	0	$\sqrt{1/49}$	0	$\sqrt{30/441}$
	±1	∓1	0	0	$-\sqrt{6/49}$	0	$-\sqrt{40/441}$
	0	0	1	0	$\sqrt{4/49}$	0	$\sqrt{36/441}$

التركيب الدقيق الموجود في Exciton-Magnon Bands لأيونات المغنيسيوم (Mn^{2+})

إن العمل المقدم في هذه الأطروحة هو دراسة الانتقالات بين المستوى $^6A_{1g}(^6S)$ والمستوى $^4T_{2g}(^4D)$ لأيونات المغنيسيوم (Mn^{2+}) في مركب $RbMnF_3$ الذي له درجة حرارة نييل (T_N) تساوي 82.6^oK. وقد لوحظ عند درجة حرارة منخفضة ظهور تركيب دقيق (Fine Structure) في D-band في مركب $RbMnF_3$. وتم مناقشة هذا التركيب الدقيق عن طريق فحص كلا من الآليات التالية : آلية التفاعل المتبادل، شريط الموجة للسبن أو امتصاص (Exciton-Magnon) ، آلية الإهتزاز، و تفاعل السبن - المدار.

وقد أظهرت التحاليل والنتائج بأن آلية التفاعل المتبادل يلعب دورا مهما في ظهور التركيب الدقيق في D-band . التغيير في الموضع الخطي في D-band يمكن دراسته إذا اعتبرنا أثر التفاعل المتبادل بين أيونات المغنيسيوم (Mn^{2+}) المتجاورة. أيضا اختفاء القمم للتركيب الدقيق في D-band فوق درجة حرارة نييل (T_N) يفسر بوساطة اضطراب السبن وتلاشي التفاعل المتبادل بين أيونات المغنيسيوم (Mn^{2+}) المتجاورة . كذلك اعتماد D-band في مركب $RbMnF_3$ على درجة الحرارة بعد درجة حرارة نييل (T_N) يثبت بأن D-band هي عبارة عن Exciton-Magnon band.